Chronic wounds are associated with inhibition of Smad3 phosphorylation

Thesis submitted as requirement to fulfill the degree
„Doctor of Philosophy“ (Ph.D.)

at the
Faculty of Medicine
Eberhard Karls University
Tübingen

by

Liu Chao

from

Zibo City, Shandong Province, China
2024

Dean: Professor Dr. B. Pichler

1. Reviewer: Professorin Dr. S. Ehnert

2. Reviewer: Professor Dr. R. Lukowski

Date of oral examination: ___02/09/2025____

Table of Contents

List of abbreviations

Alk	activin receptor-like kinase
3D	three dimensional
ANOVA	analysis of variance
BMI	body mass index
BMP	bone morphogenic proteins
bNGF	neurotrophic factor nerve growth factor
BSA	bovine serum albumin
CCL	c–c chemokine ligand
COL1A1	collagen type I alpha 1
CTGF	connective tissue growth factor
ddH_2O	double distilled H_2O
DEPC	diethyl pyrocarbonate
DMSO	dimethyl sulfoxide
ECL	enhanced chemiluminescence
ECM	extracellular matrix
EDTA	ethylenediaminetetraacetic acid
EGF	epidermal growth factor
FCS	fetal calf serum
FN	fibronectin
GAPDH	glyceraldehyde 3-phosphate dehydrogenase
G-CSF	granulocyte colony-stimulating factor
HIF	hypoxia-inducible factor
HRP	horseradish peroxidase
HUVECs	human umbilical vein endothelial cells
IGF	insulin-like growth factor
IL	interleukin
LPS	lipopolysaccharide
M-CSF	macrophage colony-stimulating factor
MMPs	matrix metalloproteinases
PBS	phosphate buffered saline
PCR	polymerase chain reaction
PDGFR	platelet-derived growth factor receptor alpha
RIPA	radioimmunoprecipitation assay
ROS	reactive oxygen species
TIMPs	tissue inhibitors of metalloproteinases
TNF-α	tumor necrosis factor alpha
UV	ultraviolet
VEGFA	vascular endothelial growth factor A
VEGFR	vascular endothelial growth factor receptor 2

1. Introduction

1.1 Epidemiology of chronic wounds

A chronic wound is an injury to the skin that cannot heal within one month or that has healed but failed to provide a sustained anatomical and functional outcome (Sen, Roy et al. 2017). The chronic wound burdens the body, emotions, and economy, both at an individual and social level.

The history of patients with chronic wounds usually lasts months or even years (Frykberg and Banks 2015). The non-healing wound means the loss of the skin's protective barrier, which directly exposes the wound to the air. This exposure increases the risk of infections and the continuous loss of water and nutrients. So, patients with chronic wounds have a low life quality and show high morbidity and mortality rates (Richmond, Maderal et al. 2013). Chronic wounds lead to limited mobility, limb pain, and serious stress on emotion. In patients with chronic wounds, depression is a highly common comorbidity. At least 30% of those patients experience symptoms of anxiety or depression (Renner and Erfurt-Berge 2017).

A chronic wound is also a heavy burden to the public health system and society. Chronic wounds are estimated to affect 1.51- 2.21% of people worldwide (Martinengo, Olsson et al. 2019). In Germany, the percentage of residents with chronic wounds was 7.8% from 2012 to 2018, with increasing incidence and prevalence every year (Raeder, Jachan et al. 2020). An individual chronic wound cost was 9,060 € on average per year, including medical insurance and personal payment (Velickovic, Szilcz et al. 2022). With increasing incidence and prevalence, spending on chronic wounds will increase and the burden on patients and society will become much heavier.

So far, despite various therapeutic approaches to chronic wounds, it is still unclear how chronic wounds develop, especially on a molecular level. Therefore,

our purpose was to explore the mechanisms behind the development of chronic wounds and to identify treatment options.

1.2 Skin anatomy

Our body is entirely covered in skin which protects it from harm. Three layers of the skin are the subcutaneous layer, dermis, and epidermis (Figure 1). The outmost layer is the epidermis, which mainly includes keratinocytes. Under this layer, is the dermis, which is primarily composed of fibroblasts. It helps in thermoregulation, sensitivity, and supports and protects deeper parts of the skin. The lowest layer of skin is named subcutaneous layer, composed of fat tissue. It insulates the body, stores energy, and connects the skin to muscles and bones. These three layers comprise the complete skin and are the body's first barrier against diseases, UV radiation, toxins, and mechanical harm (Eyerich, Eyerich et al. 2018).

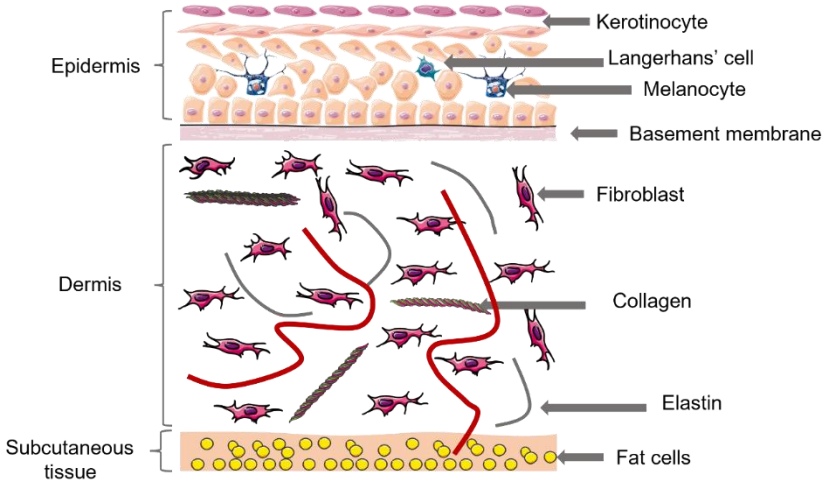

Figure 1: Schematic of human skin anatomy and types of cells. Two main human skin layers: are the epidermis and dermis. In the top layer, mainly keratinocytes, and a few Langerhans cells and melanocytes are found. In the dermis, mainly fibroblasts, collagen, and elastin are found. The subcutaneous tissue layer is mainly comprised of fat cells (Zhang, Abbasi et al. 2019).

1.2.1 Epidermis

Keratinocytes, which comprise most of the epidermis, are generated from the ectoderm and constantly regenerate the skin's outermost avascular layer (renewed approx. every 30 days), which keeps the skin barrier properties intact. Epithelium consists of five layers: superficial, subdermal, granular, spinous, and basal.

Stratum corneum is on the top, which contains keratin and horny scales formed by decomposing keratinocytes (Yousef and Sharma 2017). This layer varies most in thickness, especially in callused skin. This layer serves as the body's contact with the outside environment. It is well known for serving as a barrier to keep undesired items out and excessive water loss from occurring (Menon, Cleary et al. 2012). The defensins released from the dead keratinocytes in this layer function as our first line of immunological defense (Yousef and Sharma 2017).

The stratum lucidum is a thin, transparent layer with a thickness of 2-3 cells exclusively seen on thick skin (palms and soles). A uniform layer of keratinocytes without nuclei or other organelles makes up this layer. Its purpose is to safeguard vulnerable areas from harm (Yousef, Alhajj et al. 2022).

The stratum granulosum comprises three to five layers of cells comprising lamellar and keratohyalin particles. The proto-keratins aggregate and crosslink to form bundles within keratohyalin granules. The glycolipids in lamellar granules can be secreted on the cell membrane to function as a binding agent to keep the cells together (Yousef, Alhajj et al. 2022).

Eight to ten layers of irregular, polyhedral keratinocytes which make up the stratum spinosum are actively dividing. Desmosomes, which are clingy proteins, hold the cells together. This layer causes keratinization and keratin production. The Langerhans cells, which act as macrophages by absorbing bacteria, foreign

objects, and injured cells that arise in this layer, are also found among the keratinocytes. Our skin becomes more potent and flexible through the *stratum spinosum* (Yousef and Sharma 2017).

The foundation membrane (basal lamina) divides the stratum basale from the dermis. Hemidesmosomes bind the stratum basale to the basement membrane. In this layer, active stem cells constantly produce keratinocytes. In addition to acting as the progenitor cell layer, the basal cell layer also creates the basement membrane, the point at which the epidermis and dermis connect (Scott and Miller 2003). Melanocytes and Merkel cells are located in this layer.

1.2.2 Cells of Epidermis

Cells in the epidermis are classified into four types: keratinocytes, Merkel cells, Langerhans cells, and melanocytes.

About 90% of cells in the epidermis are keratinocytes, which start from the stratum basale, and advance to the stratum corneum. In the stratum basale, keratinocytes multiply and differentiate gradually as they move toward the surface. This kind of differentiation is regulated by changes in the environment and epigenetic modifications. During this process, they undergo significant morphological changes, and keratin, cytokines, growth factors, interleukins, and complement factors are produced (Lee 2015). At the same time, keratinocytes interact with other skin cells.

Melanocytes, originating from neural crest cells, create melanin, the pigment that gives skin its color. They are situated among the cells of the stratum basale.

Langerhans cells in the stratum spinosum involve the initial line of defense.

Merkel cells which work as mechanoreceptors are in the layer of stratum basale. They are primarily found on the oral and vaginal mucosa, fingertips, palms, and soles (Yousef, Alhajj et al. 2022).

1.2.3 Dermis

The dermis is under the epidermis layer. It helps in thermoregulation, sensitivity, and support and protection of deeper layers of skin. The papillary and reticular layers make up the dermis layer. The above is a papillary layer that contains loose connective-tissue. This layer comprises type III collagen, elastic fibers, and a capillary loop that can provide blood to the epidermis. The epidermis and superficial dermis's temperature are likewise managed by this capillary network (Green, Mansfield et al. 2014). The reticular layer is more profound, denser, and less cellular, composed of thick bundles of connective tissue and collagen fibers. The mechanoreceptors *Ruffini corpuscles*, which are in charge of sensing mechanical pressure and distortion, are located in this layer. The normal structure and function of the dermis are dependent upon the presence of important cells, namely mast cells, adipocytes, fibroblasts, and histiocytes.

1.2.4 Subcutis

The subcutis is the home of adipose tissue and a few skin appendages are located here, including blood vessels, sensory neurons, and hair follicles. The dermis anchors to the deep fascia by collagen and elastic fibers of this region. Subcutaneous fat protects from injury and cold temperatures (Ahn and Kaptchuk 2011). *Pacinian corpuscles*, which serve as the layer's mechanoreceptors, provide this layer with vibration and pressure sensations (Zimmerman, Bai et al. 2014).

1.3 Wound classification.

A wound is the loss of continuity of the skin and mucous membranes due to injuries. Injuries such as direct or indirect force, burns, paper cuts, skin tears, or surgical operations may result in wounds, so wounds can be classified according to the injury causes. Wound types are also related to comorbidities of

the patients, like diabetes, vascular diseases, dermatitis, tumors, and tuberculosis, which can affect the development of wounds (Beyene, Derryberry et al. 2020). Thus, the treatment of comorbidities is essential for the healing of wounds.

Wounds are generally classified into chronic wounds and acute wounds according to the duration the wound lasts. In general, the duration of wound healing depends on the type of wound or its location. Acute wounds often undergo an ordered, quick healing process, leading to a long-lasting restoration of anatomical and functional integrity in four weeks. However, if a wound does not go through all stages of healing, it will eventually become chronic. Chronic wounds are presumed to be those that do not heal and do not exhibit any evidence of recovery after four weeks (Zeng, Macri et al. 2017). Most chronic wounds are decubitus, diabetic ulcers, venous ulcers, and infected wounds (Gould, Abadir et al. 2015). 1-2% incidence of chronic wounds in developed countries makes a heavy burden on healthcare systems and socioeconomy (Järbrink, Ni et al. 2016). Worst of all, chronic wounds increase the morbidity and mortality of patients. Therefore, future research must focus on developing more potent therapies for chronic wounds.

1.4 The healing process of a wound.

Wound healing includes bleeding, coagulation, inflammatory response, cell regeneration, migration and proliferation, extracellular matrix formation, and remodeling (Labler, Mica et al. 2006, Rivera and Spencer 2007). This healing process is continuous and partially overlapping and can be divided into different phases (Richardson 2004). The healing process begins immediately after an injury. Four steps, including hemostasis, inflammation, proliferation, and remodeling, comprise the whole wound-healing process (Figure 2).

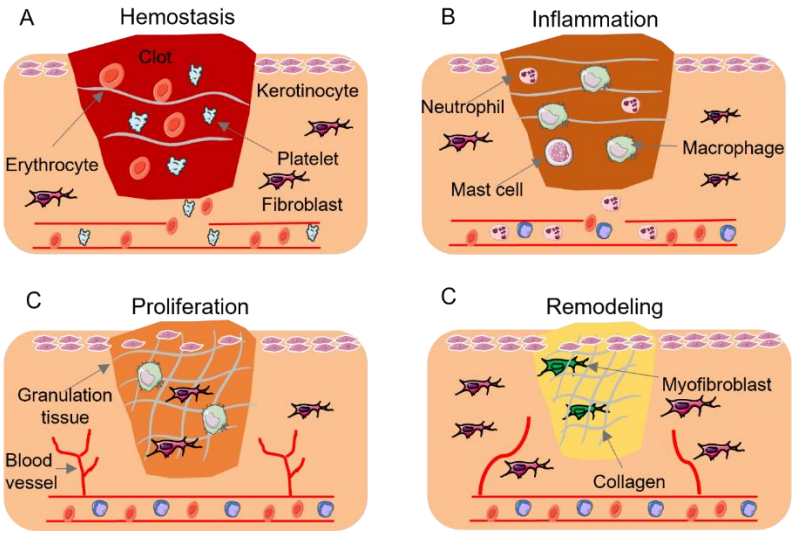

Figure 2: Phases of wound healing. (A) Hemostasis, (B) Inflammation, (C) Proliferation, (D) Remodeling. (Wilkinson and Hardman 2020)

1.4.1 Hemostasis

After the injury, blood vessels rupture, then platelets are activated by exposed collagen, and the coagulation cascade starts with clotting factors from the wound. At the same time the injured arteries undergo a 5- to 10-minute vasoconstriction (Martin 1997). The wound is filled with a clot of blood which is made of thrombospondins, fibrin molecules fibronectin, and vitronectin (Reinke and Sorg 2012). The provisional matrix of the blood clot serves as a scaffold where keratinocytes, fibroblasts, endothelial cells, and leukocytes can migrate and as a repository of growth factors. Platelets in the blood clot release chemotactic proteins to increase leukocyte infiltration. Growth factors and cytokines released by platelets and leukocytes promote an inflammatory response whereby an inflammatory phase starts.

1.4.2 Inflammatory phase

This phase begins at the end of the hemostasis phase and usually takes two days. Its main goals are establishing an immunological defense against invasive

bacteria, eliminating pathogens and necrotic tissue, and preparing the wound bed to form new tissue. Within 24 to 36 hours of injury, neutrophils reach the wound through the blood leaking from the damaged blood artery. Neutrophils can be attracted to the wound by certain cytokines, chemokines, and bacterial endotoxins which act as chemoattractants (Kolaczkowska and Kubes 2013). Neutrophils destroy necrotic tissue and infections by phagocytosing them and producing reactive oxygen species (ROS), proteolytic enzymes and antimicrobial peptides (Segel, Halterman et al. 2011).

Circulating monocytes infiltrate the wound tissue 48–72 hours post-injury when they respond to the local milieu by differentiating into macrophages. Numerous chemoattractive substances, such as clotting factors, complement factors, and cytokines, guide macrophages to the wound site. This is of special importance as monocytes and macrophages have a longer life span than neutrophils (Velnar, Bailey et al. 2009). Macrophages are the key regulatory cells within the inflammatory phase, producing large amounts of tissue growth factors and other mediators that activate keratinocytes, fibroblasts, and endothelial cells (Velnar, Bailey et al. 2009).

1.4.3 Proliferative phase

Re-epithelialization, extracellular matrix formation, and angiogenesis are characteristics of the proliferative healing period. In this period, keratinocytes, macrophages, endothelial cells, and fibroblasts are activated and work together to close the wound. As early as 12 hours after damage, local changes in electrical gradients and mechanical tension can activate keratinocytes (Shaw and Martin 2016). Due to this activation, keratinocytes at the front can move over the wound to reestablish the top layer of the skin, which induces partial epithelial-mesenchymal transition in keratinocytes at the wound edge (Wager and Leavesley 2015). Superbase keratinocytes near the leading edge transform

into leading cells when they migrate up on top of basal keratinocytes. Keratinocytes go through terminal differentiation following total basement membrane reformation to regenerate and stratify the epidermis (Baum and Arpey 2005). In addition, keratinocytes can produce extracellular matrix components such as collagens, laminins, and proteoglycans, which contribute to forming a provisional matrix (Pfisterer, Shaw et al. 2021). During matrix formation, keratinocytes secrete many growth factors and cytokines, which can also help regulate ECM formation (Ansel, Perry et al. 1990). At the same time, ECM can control angiogenesis by acting as a signaling component and supporting layer (Li, Zhang et al. 2003).

1.4.4 Remodeling phase

In this phase, it begins a few weeks later and lasts for at least a year after the injury. This phase primarily includes the production of scar tissue and new epithelium. During this phase, fibroblasts produce fibronectin, mature collagen fibrils, proteoglycans, and hyaluronan to replace the previous fibrin clot (Darby, Laverdet et al. 2014). Collagen III comprises most granulation tissue, but collagen I takes some places as the wound remodels. But the components of adult skin are mainly collagen I (80%) with only a small amount of collagen III (15%) (Campos, Santos Junior et al. 2023). Collagen III to collagen I ratio changes with time in the remodeling phase, eventually close to the ratio in normal skin.

It's very hard to completely regain the same structure and integrity of healthy skin with scars. Following an injury, wound scar tissue only restores 80% of its pre-wounding strength (Witte and Barbul 1997, Young and McNaught 2011). Scar formation depends largely on the synthesis and degradation of collagen and a fine equilibrium between the production and breakdown of collagen is required for subsequent changes to ECM. This equilibrium is maintained by

controlling the timing of essential MMPs produced by keratinocytes, fibroblasts, and macrophages. Inhibitory elements, like TIMPs closely control and synchronize their activity. TIMPs start to block MMPs after ECM is altered, preventing further ECM degradation. Chronic wounds and aberrant ECM alteration can result from an imbalance in TIMP and MMP expression (Saarialho-Kere 1998).

1.5 TGF- β and the TGF- β signaling pathway.

1.5.1 TGF-β superfamily

In this family, the primary members are TGF-β1-3, activins, and bone morphogenic proteins (BMP). TGF-β1-3 are the three primary members of TGF-β family discovered in mammals. TGF-β can control proliferation and migration, differentiation, extracellular matrix (ECM) formation, and immunological regulations (Penn, Grobbelaar et al. 2012) (Figure 3). TGF-β1-3 is secreted in its inactive form. The N-terminal latency-associated peptide forms a non-covalent connection with the C-terminal mature TGF-β (Annes, Munger et al. 2003). Thrombospondin-1, low PH, proteases, reactive oxygen species, and shear stress can activate these latent forms to release the mature, physiologically active growth factor (Worthington, Klementowicz et al. 2011). Three TGF-β isoforms play different roles at different stages. In the healing of cutaneous wounds, TGF-β1 predominates, it is promptly released upon acute injury mainly by keratinocytes and platelets (Barrientos, Stojadinovic et al. 2008). Early on, inflammatory cells like neutrophils, lymphocytes, and macrophages are attracted to the wound by the released TGF-β1 (Crowe, Doetschman et al. 2000). These immune cells are essential for tissue debridement. Once the immune cells are activated, TGF-β1-mediated repression can stop the inflammatory process. TGF-β1 thus has a dual function on the inflammation

phase during the process of healing wounds by initially having chemoattractant effects and later helping to reduce inflammation (Finnson, McLean et al. 2013). To form the granulation tissue, TGF-β1 promotes extracellular matrix like fibronectin and collagen. TGF-β 1 is related to the production of scars due to its influence on extracellular matrix deposition (Crowe, Doetschman et al. 2000). TGF-β can also control angiogenesis in the wound by increasing some proangiogenic factors like basic fibroblast growth factor (bFGF), interleukin-1, platelet-derived growth factor (PDGF), and so on (Pepper 1997). Similar to TGF-β1, TGF-β2 attracts fibroblast and inflammatory cells to the wound lesions. TGF-β2 can induce angiogenesis, which in turn enhances the production of granulation tissue and reepithelization in an *in vivo* experiment (Barrientos, Stojadinovic et al. 2008).

TGF-β3 and TGF-β1 are generally identical, but there are still conflicting effects between them, particularly on the formation of scars. Contrary to TGF-β1, TGF-β3 inhibits fibroplasia in the healing of wounds; TGF-β1 was reported to be overexpressed in systemic sclerosis in addition to causing scarring (Lichtman, Otero-Vinas et al. 2016). Additionally, it demonstrates that TGF-β3 is a potent stimulator of neovascularization and vascular rearrangement (Barrientos, Stojadinovic et al. 2008).

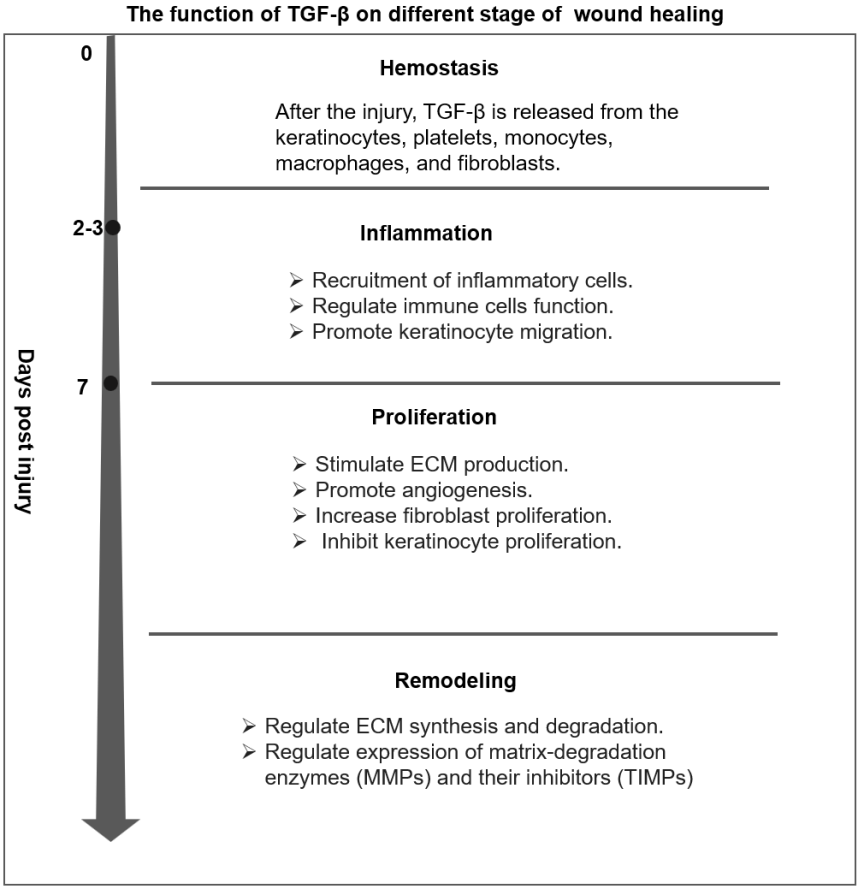

Figure 3: TGF-β function on different stages of wound healing. Wound healing process could be artificially separated into four phases following the time. During the hemostasis phase, different TGF-β isoforms are secreted into the wound; in the inflammation phase, recruit inflammatory cells, regulate the function of immune cells, and promote keratinocyte migration; on proliferation phase, TGF-β stimulates ECM production, increases fibroblast proliferation and inhibits keratinocytes proliferation; on remodeling phase, TGF-β mainly regulates ECM production and degradation.

1.5.2 TGF-β signaling pathway.

TGF-β function is completed by its signaling pathway, which maintains homeostasis of the skin and obtains skin repair after injury. Once activated, the ligand of TGF-β connects with transmembrane TGF-β receptor II (TGFβRII), which attracts a Type I receptor to form a complex with the ligand and phosphorylates the Type I receptor. Next, activated TGFβRI makes Smad2/3

phosphorylation, which transfer into the nucleus after heterodimerization with Smad4. Target genes of TGF-β are expressed under the supervision of transcriptional regulators, which are activated Smad complexes in the nucleus (Figure 4). TGF-β promotes expression of Smad6 and Smad7, inhibiting nuclear translocation and phosphorylation of Smad2 and Smad3. Pathological scarring during wound healing also shows a result of dysregulated TGF signaling (Kiritsi and Nystrom 2018). However, as the TGF-β signaling pathway is context-dependent, its particular role in chronic wounds is still unclear (Kiritsi and Nystrom 2018). So, exploring the mechanism of TGF-β signaling pathway in chronic wounds is the aim of this thesis.

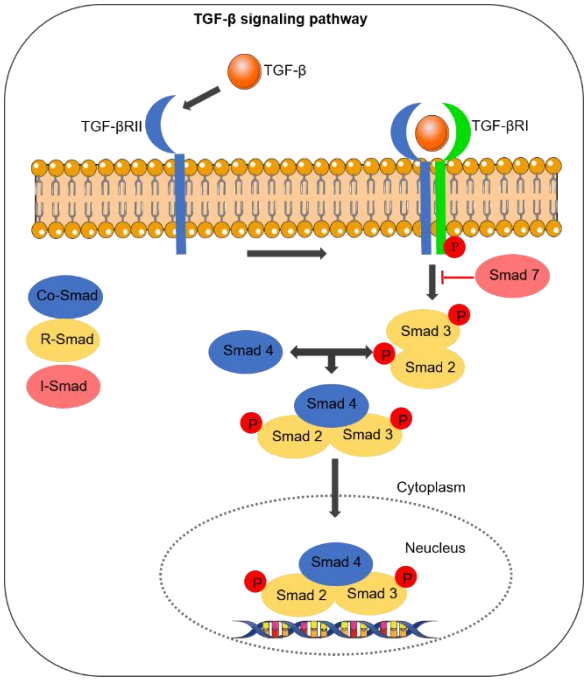

Figure 4: Cascade of the canonical signaling pathway of TGF-β. Following Smad2/3 phosphorylation, the complex formation of pSmad2/3 with Smad4 will go through into the nucleus and induce target genes' transcription. Smad7 could produce an inhibitory effect on TGFβR1 to block this signaling pathway (Chung, Chan et al. 2021).

1.6 Wound model for research

Wound models are critical to wound research. Whether it is to explore the molecular mechanism of wound healing or to develop new therapeutic methods, a model that perfectly fits the wound is needed. Recently, different kinds of wound models have been developed, including *in silico*, *in vivo*, and *in vitro* models (Ud-Din and Bayat 2017).

In silico models are computational models that can be utilized to create efficient scaffolds and tissue replacements that will aid in the production and healing of wounds as well as provide a theoretical understanding of cell proliferation and the stages of wound healing. However, since this model does not replicate the biophysical properties of human skin, it has to be tested using *in vivo* or *in vitro* models (Sami, Heiba et al. 2019) .

There are three main *in vitro* models: monolayer cell cultures, co-cultures, and 3D cultures (Hofmann, Fink et al. 2023). The mono-layered cultures are easy, cheap, and relatively fast in providing results. However, they cannot reflect the interaction of the different sorts of cells in the wound (Hofmann, Fink et al. 2023). The co-culture model was developed with two main types of skin cells, keratinocytes and fibroblasts (Hofmann, Fink et al. 2023). This kind of co-culture model helped to understand the keratinocytes and fibroblasts interaction and provided more insight into wound healing and scar formation, but these co-culture models didn’t involve blood cells. The published 3D models were usually produced using collagen carriers, which contained fibroblasts or some immune cells, on which the keratinocytes were seeded (Karamichos, Lakshman et al. 2009). Finally, the wound was formed by a biopsy punch. Although this kind of 3D model includes primary cells contained in the wound, it cannot produce the corresponding wound environment (Karamichos, Lakshman et al. 2009).

Animal models are the most widely used models; various aspects of wound healing can be investigated in a reproducible, controlled environment. Animal models are also suitable for many skin disorders and diseases. However, the use of animal models is constrained by various skin kinds, drawn-out production methods, high prices, and moral considerations (Hartung 2008). The interaction produced by skin and blood cells in the scab determines the stages of wound healing. Without the blood cells, this interaction cannot be detected.

Considering the lack of *in vitro* models of skin cells and blood cells interacting together, the ideal wound model should be stable and able to represent human skin, reflect how skin cells and blood cells interact in wound healing process, and the model is not complicated and economic. Therefore, in our study, we made use of HaCaT cells and fresh blood to produce an in vitro scab model capable of responding to early wound phases.

1.7 Study Aim

In this study, our purpose was to investigate the molecule mechanism of chronic wounds, and then hopefully to find a novel treatment target. To achieve this purpose, the following tasks were completed:

- Investigation of molecule mechanisms of chronic wounds
  - Collection of patients' samples.
  - Explore the possible targets of chronic wounds.
  - TGF-β signaling pathway in chronic wounds.
- Establishment of an *in vitro* model:
  - Characterization of this *in vitro* model.
  - The effect of exogenous TGF-β1 on this *in vitro* scab model.

2. Materials and Methods

2.1 Materials

2.1.1 Chemicals and reagents

Substance	**Article No.**	**Company**
2-Mercaptoethanol	4227.3	Carl Roth
30% hydrogen peroxide solution	CP26.5	Carl Roth
Agarose	2267.4	Carl Roth
Alk5 inhibitor	13031	Cayman Chemical
Antibiotic/Antimycotic stock solution	P-11002	PAA
Acetic acid	20104.298	VWR
Acrylamide- Bisacrylamide Solution (30%)	3029.2	Carl Roth
Ammonium Persulfate	9592.2	Carl Roth
Ammonium Thiocyanate	221-988-100	Sigma
Bovine Serum Albumin (BSA)	8076(4)	Carl Roth
Brij 35	CN21.1	Carl Roth
Bromophenol	A152.2	Carl Roth
Bromphenol Blue	A512.2	Carl Roth
Calcium chloride ($CaCl_2$)	CN93.1	Carl Roth
Calcein acetoxymethyl ester (calcein AM)	ABD (220-02)	ATT Bioquest
Copper (II)-sulfate-pentahydrate (CuSO4)	P024.1	Carl Roth
Deoxycholic acid (DOC)	3484.1	Carl Roth
Dimethylsulfoxide (DMSO)	CN93.1	Carl Roth
Dulbecco's Phosphate Buffered Saline (DPBS)	95230	Sigma
DMEM with phenol red (10X)	D5796	Sigma
Endothelial Cell Growth Basal Medium 2 (EGM-2)	C-22211	Promo Cell
Ethylenediaminetetraacetic acid (EDTA)	8043.2	Carl Roth
Ethanol (EtOH)	4720.2	Carl Roth
Ethidium bromide (1%)	2218-1	Carl Roth
Fetal Bovine Serum (FCS)	D8537	Sigma
Folin's Reagent	F9252	Sigma

Substance	Article No.	Company
Formaldehyde solution (37 %)	A1613	Applichem
Gelatin	41G7141K	Invitrogen
Glutardialdehyd	4979.1	Carl Roth
Glycerin	G7041	Sigma
Glycin	3778.1	Carl Roth
Glycine	7530.1	Carl Roth
Guanidine Thiocyanate	0017.1	Carl Roth
HCl conc.	N076.1	Carl Roth
HEPES	3908.2	Carl Roth
Hoechst 33342	3908.2	Carl Roth
human VEGFA165	C-64420A	Promokine
human Epidermal growth factor (EGF)	C-60170	Promokine
hrIGF-R3	C-60839	Promokine
Hydrocortisone		Pfizer
Hydrogen chloride (HCl) 4 M	HN78.2	Carl Roth
Hydroxyapatite	14533-100MG	Sigma
Isopropanol	33539	Honeywell
L-ascorbic acid	A7506-25G	Sigma
Leupeptin	CN33.2	Carl Roth
L-Ascorbic acid-2-phosphate sesqui-magnesium salt	21223	Sigma
Luminol	4203.1	Carl Roth
Magnesium chloride (MgCl2)	33539	Honeywell
MEM α	A8960-5G	Sigma
Methanol	KK36.2	Carl Roth
Na-K-Tartrate	S2377	Sigma
Na2CO3	P028.1	Carl Roth
Para- Nitropheyl-Phosphate (pNPP)	32213	Honeywell
p-Cumaric acid	9908.1	Carl Roth
Pepstatin A	P4265-5MG	Sigma
Penicillin/Streptomycin (p/s)	P0781	Sigma
pH indicator Pehanon	90417	Macherey-Nagel
Phenylmethylsulfonyl fluoride (PMSF)	6367.1	Carl Roth
Poncau S	5938.2	Carl Roth
Resazurin sodium salt	4165.1	Carl Roth

Substance	Article No.	Company
Roti-Mark BICOLOR	2806.2	Carl Roth
Roti Aqua Phenol	A980.3	Carl Roth
RPMI 1640	AB120297	Abcam
Sodium Dodecyl Sulfate (SDS)	CN30.2	Carl Roth
Sodium fluoride (NaF)	P756.1	Carl Roth
Sodium orthovanadate (Na3VO4)	S6508-10G	Sigma
Sodium hydroxide (NaOH)	R8758	Sigma
Sodiumacetate	CN30.2	Carl Roth
Sodiumchloride (NaCl)	T135.1	Roth
Sulforhodamine B sodium salt	X891.2	Carl Roth
Tetramethylethylenediamine (TEMED)	S7653	Sigma
Tergitol Solution	NP40S-100 ml	Sigma
TGF-β1	1218209	PerproTech
TGF-β2	0321345	PerproTech
TGF-β3	0613410	PerproTech
TRIS	T1503-1KG	Sigma
Triton-X-100	T1503- 1KG	Sigma
Trypsin/EDTA	T3924	Sigma
β-Glycerophosphate disodium salt hydrate	T3924	Sigma

2.1.2 Buffers, medium, and solutions

Buffers/Mediums/Solutions	**Compounds and handling**
Acetic acid solution (1%)	500 µl Acetic acid 49.5 ml ddH_2O
BSA blocking buffer (5%)	0.5 g BSA 50 ml DPBS
Brij 35 solution (1%)	1 g Brij 35 100 ml ddH_2O
CuSO4 Stock Solution	1 g $CuSO_4*5H_2O$ 100 ml ddH_2O
Calcein AM stock solution	502 µl DMSO 1 mg Calcein AM
Electrophoresis buffer (5X)	75 g Glycine 15.17 g TRIS 5 g SDS Adjust volume to 1 l with ddH_2O
Electrophoresis buffer (1X)	200 ml Electrophoresis buffer 5X 800 ml ddH_2O
Formaldehyde solution (4 %)	12 ml 37 % Formaldehyde solution 88 ml DPBS
HaCat medium	500 ml DMEM 5 ml Penicillin/Streptomycin 25 ml Fetal Bovine Serum (FCS / heat inactivated)
Hoechst stock solution	10 mg Hoechst 33342 5 ml DMSO
HUVECs medium	500 ml EBM-2 5 ml Antibiotic/Antimycotic 10 ml Fetal Bovine Serum (FCS / heat inactivated) 250 ng human VEGFA165 5 µg human FGF-b 2.5 µg human Epidermal growth factor (EGF) 10 µg IGF-R3 11.25 mg Heparin 100 µg Hydrocortisone 500 µg L-ascorbic acid
Luminol Solution	250 mM Luminol in DMSO
Lämmli Loading Buffer 5x	300 mM Tris pH 6.8 50% Glycerol 5 mM EDTA 10% SDS 0.05% Bromphenol Blue 12.5% 2- Mercaptoethanol

Buffers/Mediums/Solutions	Compounds and handling
Na2CO3 Stock Solution	20 g Na2CO3 950 ml ddH_2O 50 ml 2 M NaOH
Na-K- Tartrate Stock Solution	2 g Na-K-Tartrate 100 ml ddH_2O
Ponceau S Solution	0.1% Ponceau S in 1% acetic acid solution-
p-Coumaric Acid Solution	90 mM p-Coumaric acid in DMSO
Resazurin stock solution (11X)	12.5 mg Resazurin sodium salt 50 ml DPBS
Roti- Blue Staining Solution (1X)	20 ml Roti- Blue (5X) 20 ml Methanol 60 ml ddH_2O
RIPA Buffer	10 mM TRIS Base, 100 mM NaCl, 0.5% Tergitol, 0.5% DOC, 10 mM EDTA, 1 µg/mL Pepstatin A, 5 µg/mL Leupeptin, 1 mM PMSF, 5 mM Sodium fluoride, 1 mM Sodium orthovanadate
Sulforhodamine B solution	0.2 g Sulforhodamine B Adjust volume to 50 ml with 1 % acetic acid
TBS 10x (Tris-buffered saline)	100 mM TRIS, 1.5 M NaCl in ddH_2O, pH=7.6
TRIS (1.5 M) for zymography	181.7 g TRIS 900 ml ddH_2O Adjust pH to 8.8 Adjust volume to 1 l with ddH_2O
TRIS (1 M) for zymography	121.1 g TRIS 800 ml ddH_2O Adjust pH to 6.8 Adjust volume to 1 l with ddH_2O
Triton-X-100 solution (2.5%) for zymography	25 ml Triton-X-100 1 l ddH_2O
Trypan blue solution	62.5 mg Trypan blue 50 ml Dulbecco's PBS
Western Blot Transfer Buffer	25 mM Tris 192 mM Glycine 20% Methanol

Buffers/Mediums/Solutions	Compounds and handling
Zymography developing buffer	6.05 g TRIS 8.766 g NaCl 1.47 g CaCl2 20 ml 1 % Brij 35 solution Set the volume with ddH_2O to 1 L
Zymography sample loading buffer (3x)	0.2 g SDS 1 g Glycerin 1 mg Bromphenol blue Set the volume with ddH_2O to 10 ml

2.1.3 Consumables

Consumable	Manufacturer	Type	Serial number
Cell culture plate	Greiner Bio-One GmbH	Flat bottom, 96 wells	655161
	Greiner Bio-One GmbH	V bottom ,96 wells	651101
	Corning Co.Ltd	Flat bottom, 48 wells	3548
	Greiner Bio-One GmbH	Flat bottom, 24 wells	662160
	Corning Co.Ltd	Flat bottom, 6 wells	353046
Cell Star Tubes	Greiner Bio-One GmbH	V bottom ,50 ml	227261
	Greiner Bio-One GmbH	V bottom ,15 ml	188271
Reaction tube	Sarstedt ag & co. kg	White, 0.5 ml	72.699
	Carl Roth	White ,1.5 ml	4182.1
	Carl Roth	Blue,1.5 ml	4190.1
	Carl Roth	Green, 1.5 ml	4209.1
	Carl Roth	Red, 1.5 ml	4189.1
	Carl Roth	Yellow, 1.5 ml	4204.1
	Eppendorf	White, 2.0 ml	2549
Pipette Tips	Sorenson BioScience	Colorless, 0.1 µl, 10 µl	
	Sarstedt	Yellow, 2 - 200 µl	
	Ratiolab	Blue, 100 - 1000 µl	
Single-channel Pipette	Corning Co.Ltd	10 µl, 100 µl	158240031
	Corning Co.Ltd	20 µl, 200 µl	158250088
	Corning Co.Ltd	100 µl, 1000 µl	058261237
	Eppendorf	0.1 µl, 2.5 µl	P35434B
Spectrophotometer	BMG Labtech	Fluostar Omega	415(1264)
Water-bath	LAUDA GmbH	Al-25	LCB-0727-11-0094
	LAUDA GmbH	ECOET (20)	LY 06-1

2.1.4 Equipment

Equipment	Manufacturer	Type	Serial number
Agitator, magnetic stirrer	IKA-Werke	RHB-2	06-05-03-57
	Heidolph	MR-Hei-Mix-L	040-700-340
Centrifuge	Dako	Stat-Spin	620E-5000-0693
	Thermo Fisher	Megafuge (40R)	4130-7652
	Scientific Industries	SIDD (58)	DD-58-1001
Microcentrifuge	Labnet International GmbH	BN-0806-0235	C-1301B
	HERAEUS	Fresco (17)	4125-0019
Electrophoresis power supplies	Bio-Rad	Power Pac (200)	285B-R05-538
Freezer -20℃	B/S/H	IQ-500	GS-51-NYW-41 (01)
	Liebherr GmbH	Med-Line	LGex-3410-21K-001
Freezer -80 ℃	Thermo Fisher	905	827-860-2521
	Revco GmbH	ULT-1386-9V17	R10G-3330-95RG
Fridge +4 ℃	Liebherr GmbH	Comfort	3523 (21L)
	Cool Compact Kühlgeräte GmbH	HKMT (04001)	CC-0041-2514
Ice maker	Scotsmen GmbH	AF (80)	DD-8837-11X
Incubator	Thermo Fisher	Heratherm OMS-60	4129-6334
	Binder GmbH	90-40-00-78	11-22-649
Laboratory pump (Bench)	Carl Roth	Cyclo-2	11-090-65
Microscope	Peqlab Biotechnologie	EVOS (fl)	91-AF-43-01
	Logos Biosystems	CELENA-X	CLX-01-00045
Mixer	Labinco B.V.	LD (76)	76-000
Multichannel Pipette	Corning Co.Ltd	5 µl, 50 µl	151-620-022
	Corning Co.Ltd	20 µl, 200 µl	551-630-277
	Thermo Electron	0.5 µl,10 µl	CH98998(4510)
	Corning Co.Ltd	50 µl, 300 µl	151640033
pH meter	Mettler Toledo	Five Easy (FE-20)	1232-3152-96
Pipette controller	Integra	Pipetboy-acu	629-619
	Heathrow Scientific	Rota-Filler-3000)	HAS-05119
Refrigerator	Cool Compact Kühlgeräte GmbH	HKMT-04001	CC-0041-2516
	Cool Compact Kühlgeräte GmbH	HKMN-062-01	CC-0041-2513

Equipment	Manufacturer	Type	Serial number
Safety Work Bench	Thermo Fisher	Maxisave-S202018	41293949
Scale	Kern &Sohn	ABJ-120-4M	WB-114-0084
Shaker, laboratory	PeqlabBiotechnolog	ES (20)	010111-1107-0119
	LTF Labortechnik	DRS-12	11DE-090
	Corning Co.Ltd	LSE (Vortex and Mixer)	110-1260
Single-channel Pipette	Corning Co.Ltd	2 µl, 20 µl	158230441
	Corning Co.Ltd	100 µl, 1000 µl	058-261-237
	Eppendorf	0.1 µl, 2.5 µl	P35-434B
Spectrophotometer	BMG Labtech	Fluostar Omega	415-1264
Shaker, laboratory	LTF Labortechnik	DRS (12)	11DE243
	PeqlabBiotechnolog	ES (20)	01-0111-1107-0119

2.2 Methods

2.2.1 Human samples

Following the Helsinki Declaration, all samples were obtained with the donors' informed consent. The University Hospital Tübingen's Ethics Committee (844/2020B02) approved the studies.
The samples were collected from patients with acute wounds (wound duration < 30 days), and chronic wounds (wound duration ≥ 30 days) after the patients gave their informed written consent. To analyze the wound healing, both wound tissue and venous blood were collected.

2.2.2 The establishment of in vitro scab models

2.2.2.1 Culture of HaCaT Cells

HaCaT cell, a spontaneously converted immortal human epithelial cell line, originally from a male patient, 62 years old, was obtained from the technical transfer service of the German Cancer Research Center (DKFZ). This keratinocyte cell line is well-established in laboratory research. It has a solid ability to differentiate and multiply in vitro. Cells were grown in T75 culture flasks using Dulbecco's Modified Eagle's Medium (DMEM) with 5% fetal calf serum (FCS). Every three to four days, the medium was changed, and after seven days, if confluent, cells were split at least 1:10.

2.2.2.2 Scab in vitro model: production and culture

This *in vitro* model was produced with HaCaT cells and fresh EDTA venous blood. The density of HaCaT cells was 0.5×10^6 cells/mL in the coagulation medium (Dulbecco's Modified Eagle's Medium (DMEM) - high glucose, 5% FCS, 7.5 mM $CaCl_2$). $CaCl_2$ was added to achieve the coagulation of the venous blood *in vitro*. A sterile 96-well plate without coating was filled with 60 µL of

blood and same volume of HaCaT cell suspension. After 1h incubation at 37 °C with 5% CO_2, the scab models were moved to a new 96-well plate and cultured in the incubators. 50 µL culture medium change was carried out every two days to maintain an ideal condition of growth (Pfeiffenberger, Bartsch et al. 2019).

2.2.3 Scab model stability and viability

2.2.3.1 Analysis of Scab Weight and Size

The measurements of weight and size were conducted immediately to avoid scab model drying after being moved into the new 96-well plate. Weight was measured by an analytical balance with at least 5 scabs at one timepoint. The scab size was evaluated by the diameter/area of the scab, which was obtained from microscopic images (1.25× magnification) analyzed with the software ImageJ 1.53m.

2.2.3.2 The evaluation of Scab Viability

Scab viability was detected by resazurin conversion. Three scabs were moved into a fresh 96-well plate and washed with PBS until the red color of the supernatant disappeared. Resazurin stock solution (11X) was diluted 1:11 in a culture medium to obtain the working solution. Each scab was incubated at 37 °C in the dark with 100 µL of resazurin working solution. After 1 hour and 2 hours, 50 µL of the supernatant was moved into a fresh 96-well plate, and the intensity of fluorescence was assessed (Ex = 544 nm; Em = 590-10 nm) using the Plate Reader (FIUO star Omega, BMG LABTECH GmbH, Germany). As a background, blank values were subtracted (Ehnert, Linnemann et al. 2018).

2.2.3.3 Viability Staining

For viability staining, scabs were moved to a new 96-well plate and incubated with 100 µL of culture medium containing 0.02 mM Calcein-AM at 37 °C in the

dark for 10 minutes. Depending on the experimental design, the GFP channel was chosen to take pictures with 20- and 40-fold magnification. ImageJ 1.53m was used to analyze the images (Haussling, Deninger et al. 2019).

2.2.4 Luciferase Assay

The adenovirus Ad5-CAGA-Luc (obtained from Prof. Peter ten Dijke), which is a Smad2/3 reporter, was used to infect HaCaT cells. Once phosphorylated Smad3/4 translocated into the nucleus luciferase expression was induced. With the SteadyGlo Luciferase Assay System, luciferase activity was evaluated with cell lysates following the recommendations of the manufacturer (Promega, Madison, WI, USA). The total protein content was used to standardize the results.

2.2.5 Gelatin zymography

Levels of MMP9, a matrix degradation marker, were measured by gelatin zymography. Culture supernatants were collected at different time points of culture. Samples, each containing 5 µL of culture supernatant and 15 µL of loading buffer (0.2 g SDS, 1 g Glycerin, and 1 mg Bromphenol blue in 10 mL double distilled H_2O) were filled into the pockets of the gelatin gel. The electrophoresis was run at 120 V for 50 minutes. 3 washing steps were done with PBS which included 2.5% Triton X-100, then 5 washing steps with ddH_2O. At 37 °C, the gel was incubated with the developing buffer for 24 hours (6.05 g TRIS, 8.766 g NaCl, 1.47 g $CaCl_2$, 20 mL 1 % Brij 35 solution in 1L ddH_2O). After staining with Coomassie blue, the signals were developed with the INTAS GelDoc system and pictures were quantified with ImageJ 1.53m (Ehnert, Seeliger et al. 2011).

2.2.6 Cytokine Array C5

To detect the cytokines in the culture supernatant of the scabs on days 1, 2, 3, 5, and 7 of culture with RayBio® Human Cytokine Array C5 (BioCat, Heidelberg, Germany). This array was conducted following the instructions of the manufacturer. A CCD camera (INTAS, Göttingen, Germany) detected the signals. The quantification of signal intensities was carried out by ImageJ software, and the normalization was done by 6 spots (positive controls) on each membrane.

2.2.7 Analysis of Gene Expression

2.2.7.1 RNA isolation

Tissue homogenization was necessary for RNA isolation. 200-500 µL of Self-made TriFast solution (9.45 g Guanidine thiocyanate, 3.04 g Ammonium thiocyanate, 3.3 mL 3 M Sodium acetate solution, 5 mL Glycerol) was added to the sample according to the volume of the sample. Samples were kept at -80 °C until additional process was done. After thawing of the sample, the same volume of Self-made TriFast solution was added as before and samples were homogenized by grinding them right away, then centrifugation was done with 14,000 g at 4 °C for 10 min after 5 min of RT incubation, and the supernatant. 100 µL chloroform (per 500 µL phenolic RNA isolation solution) was incorporated into the supernatant and blended briefly. After 8 minutes of coculture at RT, the centrifugation was conducted at 14,000 g and 4 °C for 10 minutes. Then, the upper supernatant was moved to a new Eppendorf tube containing isopropanol (50 µL isopropanol per 100 µL liquid) and was kept at -20 °C for at least 12 hours to improve the RNA yield. RNA pellets were obtained by centrifugation as defined above followed by two times washing with 1 mL of

70% ethanol. After 15 min of drying RNA pellets were resolved in 20 µL of DEPC ddH20.

2.2.7.2 RNA integrity check

RNA integrity was checked with gel electrophoresis. A 10 µL sample was produced by combining 150–300 ng of the extracted RNA with the appropriate amounts of 5X loading dye (25 mg Bromphenol blue, 5 mL 10X TBE, 5 mL 20% Glycerol). Samples were loaded in ethidium bromide-containing 1.8% agarose gels. Electrophoresis ran at 80 V for 45 minutes. Pictures were taken with the INTAS GelDoc system (Lin, Schyschka et al. 2012). Samples selected for further investigation were those exhibiting the typical 18S and 28S band patterns.

2.2.7.3 cDNA synthesis

Synthesis of cDNA was completed by the first-strand cDNA synthesis kit (Thermo Fisher). Irrespective of the reported RNA concentrations, reactions were conducted using a 4.5 µL template. The obtained cDNA was diluted to 10 ng/L. *RPL13a* and *18s* PCR were used to confirm successful cDNA synthesis, as those two genes were the most stable housekeeping genes in the in vitro scab model or patient tissue.

2.2.7.4 RT-PCR in semi-quantitative form

RT-PCR was done by a mixture including 20 µL cDNA sample, 7.5 µL Red HS Taq Master Mix, 7,5 ul former/ revers primer, and 20 µL DEPC water. Table below shows sequences of the primers and ideal conditions for RT-PCR.

Table 1: Specifications of F: Forward and R: Reverse primers used in gene expression analysis.

Primer	Forward Sequence	Reverse Sequence	cDNA (ng)	T_A (°C)	cycles	Size (bp)
18s	GGACAGGATTGACAGATTGAT	AGTCTCGTTCGTTATCGGAAT	20	56	25	111
RPL13a	AAGTACCAGGCAGTGACAG	CCTGTTTCCGTAGCCTCATG	20	56	30	100
TGF-β1	TCCGGACCAGCCCTCGGGAG	CGGTCGCGGGTGCTGTTGTA	20	58	35	680
TGF-β2	GCAGGTATTGATGGCACCTC	AGGCAGCAATTATCCTGCAC	20	58	35	206
TGF-β3	CAGCTGCCTTGCCACCCCTC	TGCAGCCTTCCTCCCTCTCCC	20	58	40	601
CTGF	CCAATGACAACGCCTCCTG	TGGTGCAGCCAGAAAGCTC	40	62	35	159
FN1	CCCCATTCCAGGACACTTCTG	GCCCACGGTAACAACCTCTT	20	60	35	203
COL1A1	CAGCCGCTTCACCTACAGC	TTTTGTATTCAATCACTGTCTTGCC	40	60	35	83
MMP1	CCCAGCGACTCTAGAAACACA	TCTTGGCAAATCTGGCGTGT	40	60	35	322
MMP2	AACATACAAAGGGATTGCCAGGA	TTCAGCACAAACAGGTTGCAG	40	60	35	117
MMP9	TCTATGGTCCTCGCCCTGAA	CATCGTCCACCGGACTCAAA	40	64	35	219
MMP13	CCTGCTGGCTCATGCTTTTC	AGACCTAAGGAGTGGCCGAA	40	64	40	141
TIMP1	AGTTTTGTGGCTCCCTGGAA	AAGCCCTTTTCAGAGCCTTG	40	60	35	179
TIMP2	ATGCAGATGTAGTGATCAGGGC	GTGATGTGCATCTTGCCGTC	40	60	35	256
Smad7	TTCGGACAACAAGAGTCAGC	AAGCCTTGATGGAGAAACC	20	60	40	200
PAI-1	CAGCTCATCAGCCACTGGAA	TGGAGAGGCTCTTGGTCTGA	40	62	40	179
VEGFA	CTACCTCCACCATGCCAAGT	GCAGTAGCTGCGCTGATAGA	40	60	40	109
Ang1	CGATGGCAACTGTCGTGAGA	CATGGTAGCCGTGTGGTTCT	40	60	35	232
VEGFR1	TCTCACACATCGACAAACCAATACA	GGTAGCAGTACAATTGAGGACAAGA	20	62	35	106
VEGFR2	CAGGGGACAGAGGGACTTG	GAGGCCATCGCTGCACTCA	20	60	32	91
IL-1α	GAATGACGCCCTCAATCAAAGT	TCATCTTGGGCAGTCACATACA	40	58	35	186
IL-1β	CTCGCCAGTGAAATGATGGCT	GTCGGAGATTCGTAGCTGGAT	40	60	35	144
IL-8	TAG CAA AAT TGA GGC CAA GG	AAA CCA AGG CAC AGT GGA AC	40	58	35	227
CCL2	CCTTCATTCCCCAAGGGCTC	GGTTTGCTTGTCCAGGTGGT	40	60	35	236
CCL5	ATCCTCATTGCTACTGCCCTC	GCCACTGGTGTAGAAATACTCC	40	60	35	135
CCL7	CTTGCTCAGCCAGTTGGGATT	CCACTTCTGTGTGGGGTCAG	40	60	35	183

2.2.8 Angiogenesis evaluation

2.2.8.1 Culture of human umbilical vein endothelial cells (HUVECs).

HUVEC medium was applied to cultivate HUVECs, which included Endothelial Cell Growth Basal Medium 2 (EBM-2). HUVECs were incubated on 0.1% Gelatin-coated flasks. There was a medium change every two to three days. For the experiments, only cells from passages 7 through 10 were employed.

2.2.8.2 Assay for Tube Formation

48-well plates were used for this experiment, and Geltrex™ (6 µL per well) (Thermo Scientific, Waltham, MA, USA) was applied in the wells for coating in advance. After the cell seeding with 6.5 × 10^4 cells per well, the respective stimulus in plain EBM-2 was incorporated into the cells. Here, pools of supernatants on three time points were used, *i.e.* time point 1: days 1, 2, and 3; time point 2; days 5, 6, and 7; time point 3: days 12, 13, and 14. Cells were cultured inside the incubator with 5% CO_2 at 37 °C for 18 hours. Staining was applied with 0.1% Calcein-AM for 10 min before checking with the microscope. After removing the staining solution, carefully washing with PBS once, and adding plain EBM-2 (200 µL per well), pictures were taken with the CELENA-X (Logos Biosystems) or EVOS fl (PeqlabBiotechnologie) imaging system in a 4X magnification. "Angiogenesis analyzer" plugin in ImageJ 1.53m was used for data analysis (Carpentier, Berndt et al. 2020)

2.2.8.3 C2 Angiogenesis array

To detect angiogenesis factors in scab, a C2 human angiogenesis array (RayBiotech, Peachtree Corners, GA, USA) was applied with the pools of supernatants described in the tube formation assay. The whole process was done as in table 2 below. An INTAS chemocam (Göttingen, Germany) was used to record the chemiluminescent signals. The software ImageJ 1.53m was used for data quantification and internal controls were used to standardize the data.

Table 2: C2 Angiogenesis array protocol.

Step	Procedure
1	Fill every well with 1 ml Blocking Buffer, and then incubate at RT.
2	Add 500 µl culture supernatant into every well and incubate at 4°C.
3	Wash membranes with Wash Buffer.
4	Incubate membranes with 1 ml of Biotinylated Antibody Cocktail (RT).
5	Wash membranes 3 times with 1 ml 1X Wash Buffer.
6	incubate membranes with 1 ml of 1X HRP-Streptavidin Solution (RT).
7	Wash membranes 3 times with 1 ml 1X Wash Buffer.
8	For chemiluminescent detection remove access wash buffer and incubate with ECL (C: D=1:1) for 1 min before taking pictures (1-30 sec intervals).

2.2.9 Immunohistochemical staining.

Skin wound tissue was fixed in 4% formalin for 12 hours, then the tissue section was dried with graded ethanol (70%, 96%, 100%) and embedded in paraffin. Paraffin-embedded wound tissue slices (3-µm thickness) were heated at 60°C for 30min, deparaffinized using Roticlear (ROTH), and hydrated again in the graded ethanol (100%, 90%, 80%, 70%, 50%). Antigen retrieval was done in sodium citrate solution (10 mM, PH=6). Blocking of endogenous peroxidase was done by using a Dual Endogenous Enzyme Block (DAKO, S2003). Primary antibody pSmad3C (IBL-28031) was applied on the slices at 4°C overnight, then secondary antibody HRP-conjugated mouse-anti-rabbit IgG (sc-2357) for 60 min at RT. Under the microscope, DAB color development time was optimized. After hematoxylin counterstaining, samples were dehydrated with graded ethanol (95%, 95%, 100%, and 100%) and mounted with DPX Mountant, and

pSmad3 were noted and examined under a microscope (Logos Biosystems) at 20X and 40X magnification. The quantification was done by ImageJ.

2.2.10 Western Blot

2.2.10.1 Isolation of protein

Small portions of the patient's wound tissue were sliced up and placed in an Eppendorf tube and covered with 250- 500 µL RIPA working solution (1 µL Pepstatin A Stock Solution, 1 µL Leupeptin Stock Solution, 1 µL PMSF Stock Solution, 1 µL NaF Stock Solution, 1 µL Na3VO4 Stock Solution, dissolve in 500 µL RIPA stock solution). Tissue samples were homogenized by grinding, then centrifugation at 1,3000 x g for 10 minutes at 4 °C. The soluble protein-containing supernatant was moved to a separate tube and kept at -80 °C for further investigation.

2.2.10.2 Lowry assay

Total protein measurement was done by Lowry assay (Lowry et al., 1951). Initially, triplicates of 2 µL of the sample or the bovine serum albumin (BSA) standard were put on a 96-well plate. 150 µL of solution A (20 µL Na-K- Tartrate Stock Solution, 20 µL $CuSO_4$ Stock Solution, bringing to 2 mL in total with Na_2CO_3 Stock Solution) was mixed with one sample for 10 minutes. 30 µL of solution B (500 µL Folin Reagent, 1000 µL ddH_2O) was then added and mixed. After two to three hours of incubation at RT in the dark, the absorbance of 750 nm was determined, and then the concentration of protein was determined from the standard.

2.2.10.3 Western blot

Protein denaturation was achieved by incubating samples at 98 °C for 10 minutes. The following step involved loading 35 µg of protein onto a 12% bis-

acrylamide 1.5 mm thickness gel (ddH2O 4.3 mL, 1.5M TRIS (PH=8) 3.2 mL, 30% Acrylamide/Bisacrylamide 5 mL, 10% SDS solution 127.5 µL, TEMED 12,8 µL, 10% APS solution 127.5 µL) and separating it using sodium dodecyl sulfate-polyacrylamide gel electrophoresis (SDS-PAGE) for 3 hours at 100 V. Wet blot transfer was used to transfer separated protein to a nitrocellulose membrane for 3 hours at 100 mA. Ponceau S staining was applied to confirm the protein transfer, and the membrane was sliced by the size of the target proteins. The membrane was put into BSA blocking buffer (2.5 g BSA, 50 mL TBS-T washing buffer) for 60 minutes. After blocking, the primary antibody was incubated on the membrane for an entire night at 4°C (dilutions and antibodies are in Table 3). Then the secondary antibody was applied on the membrane for 2 hours, after washing and development with ECL substrate, signals of pSmad3 were captured using a CCD camera (Chemocam, INTAS, Göttingen, Germany) and an enhanced chemiluminescence (ECL) solution.

Table 3: Antibodies used for western blot and immunohistochemical staining.

Target	Isotype	Manufacture	Product Number	Dilution
pSmad3	Rabbit	Immuno-Biological Laboratories	Ser-423/425	1:50 (IHC) 1:500 (WB)
GAPDH	Rabbit	Sigma-Aldrich	G9545	1:10000(WB)
Mouse IgG	Mouse	Santa Cruz Biotechnology	sc-2357	1:50 (IHC) 1:10000 (WB)

2.3 Analytical Statistics

The statistical evaluation was done with GraphPad Prism 8.01. Data are reported as median + 95% confidence interval otherwise noted. For every experiment, the figure legends give the number of separate experiments conducted (technical replicates = n and biological replicates= N). Due to the limited sample size, it was not possible to assume a Gaussian distribution, hence the conditions are contrasted using non-parametric Kruskal-Wallis and

Dunn's multiple comparison tests. Statistical significance occurred when *the P value* was below 0.05.

3. Results

3.1 High Phospho-Smad3 level in chronic wound tissue.

To understand the mechanism of chronic wounds, patients with wounds from the BG clinic were investigated, including acute wounds (<30 days) and chronic wounds (≥30 days). Of the 40 patients included in the study, one patient withdrew from study participation. Among the remaining 39 patients, 23 patients were with chronic wounds and 16 patients were with acute wounds. Only 31 patients could be unambiguously assigned to a specific wound etiology, including 17 traumatic wounds, 5 iatrogenic wounds, 2 infections wounds, 3 pressure wounds, and 4 vascular disease-related wounds. Patients' samples included plasma, blood, and wound tissue. 22 available RNA samples were isolated from the wound tissue. 29 plasma samples were used to evaluate active levels of TGF-β. In acute and chronic wounds, the main part was traumatic wounds (Figure 5). More patient information can be found in Table 4.

Table 4: Information on patients with acute and chronic wounds.

	Acute wound	**Chronic wound**	***p*-value**
Number of donors	16	23	
Wound duration [days]	16.73± 8.20	422.0± 853.90	0.0330
Age [years]	56.88± 17.37	57.87± 18.13	0.8628
BMI [kg/m^2]	27.65± 4.71	27.43± 6.60	0.9133
Female [%]	25.00%	43.48%	>0.9999
Male [%]	75.00%	56.52%	>0.9999
Smoking [%]	37.50%	26.08%	>0.9999
Diabetes [%]	18.75%	21.74%	>0.9999

BMI: body mass index

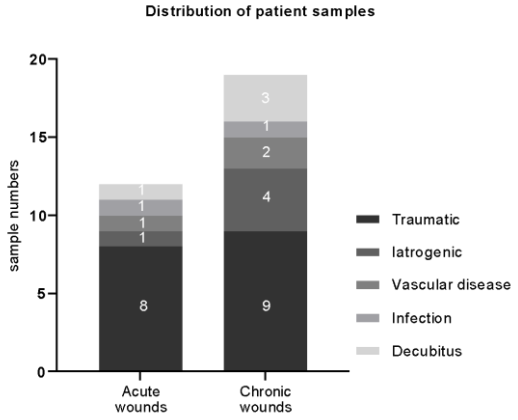

Figure 5: Distribution of wound type in acute wounds and chronic wounds.

3.1.1 High-level TGF-β in chronic wounds.

The expressions TGF-β1-3 were investigated in the wound tissue. TGF-β1 gene expression was higher in chronic than acute wounds (Figure 6A) (Ehnert, Rinderknecht et al. 2023). Lower levels of TGF-β2-3 were found in chronic wounds compared to acute wounds (Figure 6B-C). Active TGF-β1 levels were determined by luciferase reporter assay, which were lower in acute wounds (Figure 6D). TGF-β1 gene expression increased with the duration time of the wound (Figure 6E).

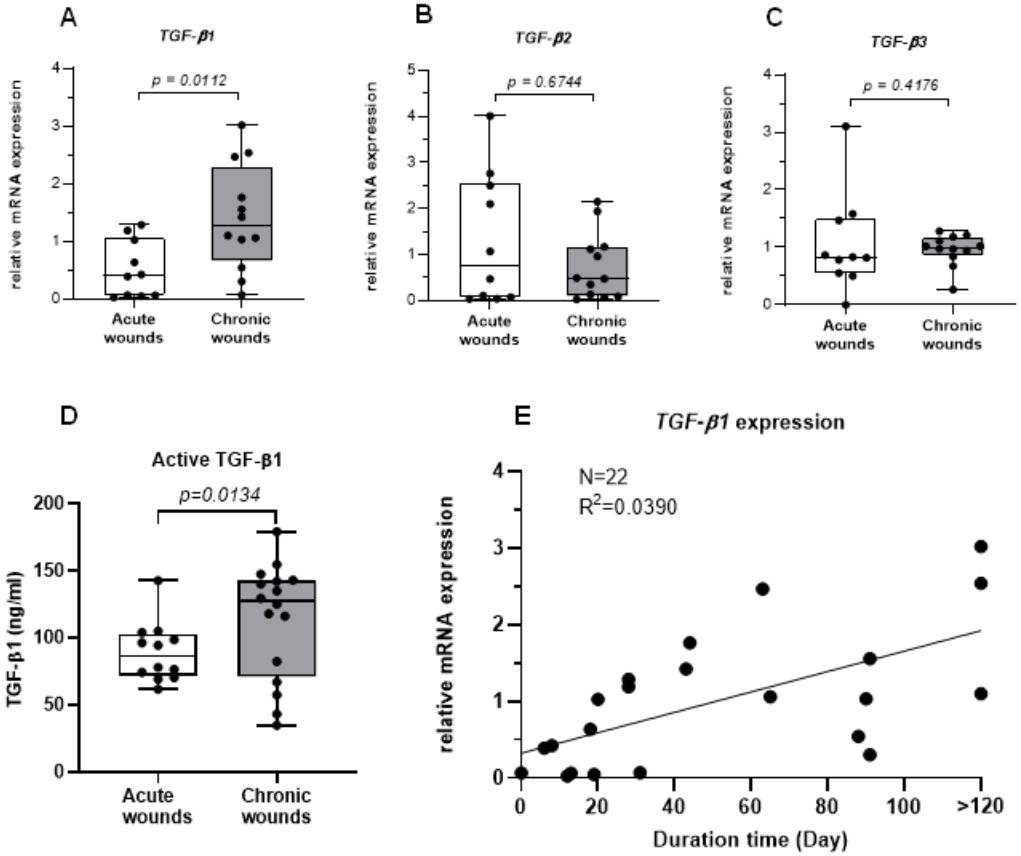

Figure 6: Three TGF- β isoforms in different wound tissues and patients' blood. RNA was isolated from the patients' wound tissue (Acute wounds: N = 10, n = 1; Chronic wounds: N = 12, n = 1), and cDNA synthesis was done, then do the RT-PCR to check the gene expression. (A-C) mRNA expression of TGF- β1-3 (D) Luciferase reporter assay was used to measure the level of active TGF- β1 in the plasma (Acute wounds: N = 13, n = 1; Chronic wounds: N = 16, n = 1). (E) The distribution of TGF- β1 according to the duration time of wounds (N =22, n =1). Data was shown as the mean ± SEM. Statistical analysis: Mann-Whitney test.

3.1.2 The impaired TGF-β signaling pathway in traumatic chronic wounds.

TGF-β1 expression in chronic wounds was higher than in acute wounds. In line with this, higher active TGF-β1 level was also detected in the plasma from patients with chronic wounds compared to patients with acute wounds (Ehnert, Rinderknecht et al. 2023). This data suggested that the TGF-β signaling pathway might be compromised. Hence, phosphorylation of Smad3 was

detected to check if the TGF-β signaling pathway is impaired or where the signaling pathway is blocked.

3.1.2.1 Higher levels of phospho-Smad3 in traumatic acute wounds.

The amount of phosphorylated Smad3 reflects the activation of this signaling pathway. Phosphorylated Smad3 in the wound tissue was evaluated by Western blot (Ehnert, Rinderknecht et al. 2023). Patient wound tissue samples were all traumatic wound tissue, including 7 acute wound samples and 8 chronic wound samples. GAPDH was the housekeeping protein to normalize the amount of pSmad3. The bands are shown in Figure 7A. Phospho-Smad3 levels were higher in acute wounds than in chronic wounds (Figure 7B).

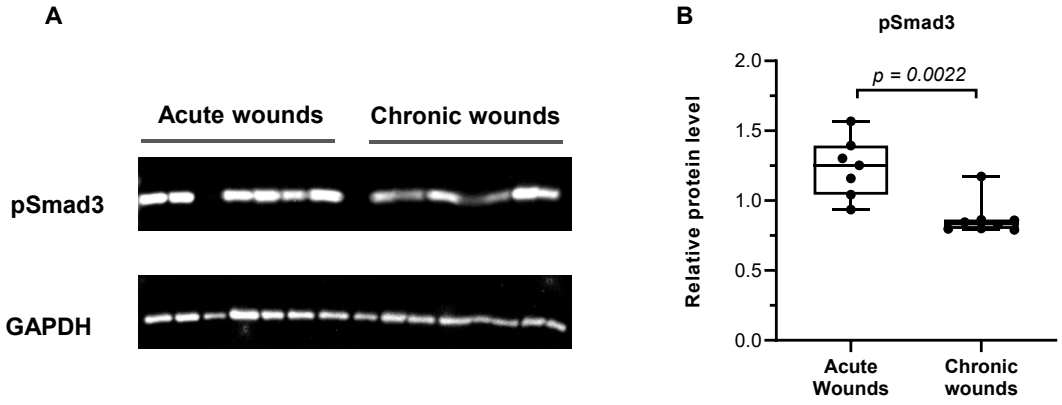

Figure 7: Western blot was used to determine the protein level. (A) The bands of phospho-Smad3 and GAPDH in acute wounds and chronic wounds. (B) Quantification of relative phospho-Smad3 level (normalized by GAPDH). Acute wounds: N = 7, n = 2; Chronic wounds: N = 8, n = 2. Box plots were used to display the data. Data was displayed by the Mann-Whitney test.

3.1.2.2 Phospho-Smad3 level was high in traumatic acute wound tissue.

Immunohistochemistry staining was used to check phosphorylated Smad3. Images illustrated that acute wound tissue had a significant increase of phospho-Smad3 in the nucleus when compared to the chronic wounds group

(Figure 8A) (Ehnert, Rinderknecht et al. 2023). With images of 40x magnification, the positive nuclei were manually counted. The result showed a higher positive percentage in acute wounds than in chronic wounds (Figure 8B), but there was no statistical significance.

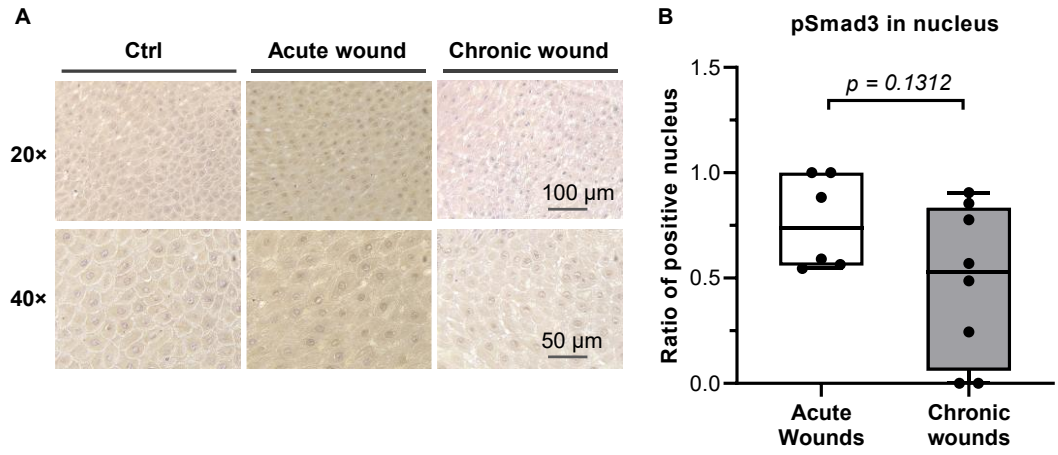

Figure 8: Immunohistochemical (IHC) staining for pSmad3 in wound tissue. (A) Representative images of IHC staining in the control group, acute wounds, and chronic wounds were recorded under 20 x and 40 x magnification. (B) Percentage of the positive nucleus in IHC staining. Acute wounds: N = 6, n = 1; Chronic wounds: N = 8, n = 1. Box plots were used to display the data. Data were shown as the mean ± SEM by the Mann-Whitney test.

3.2 Scab model development.

3.2.1 Scabs cultivated in vitro can be kept for more than 2 weeks.

Changes in scab volume and weight were used to evaluate the stability of the scabs during culture (Liu, Rinderknecht et al. 2022). Following time, the scab gradually shrunk in size and weight, and the scab turned from red to pale in color (Figure 9A, B and D). The vitality of the scab was measured by mitochondrial activity with the Resazurin conversion assay (Figure 9C). The result showed that the mitochondrial activity was upregulated at the beginning of the scab culture and after 4 days gradually decreased with time. Life-dead staining was performed to validate this finding. An increased amount of live

HaCaT cells in the scabs throughout the culture was seen by representative photos obtained on days 7, 10, 14, and 17 (Figure 9E).

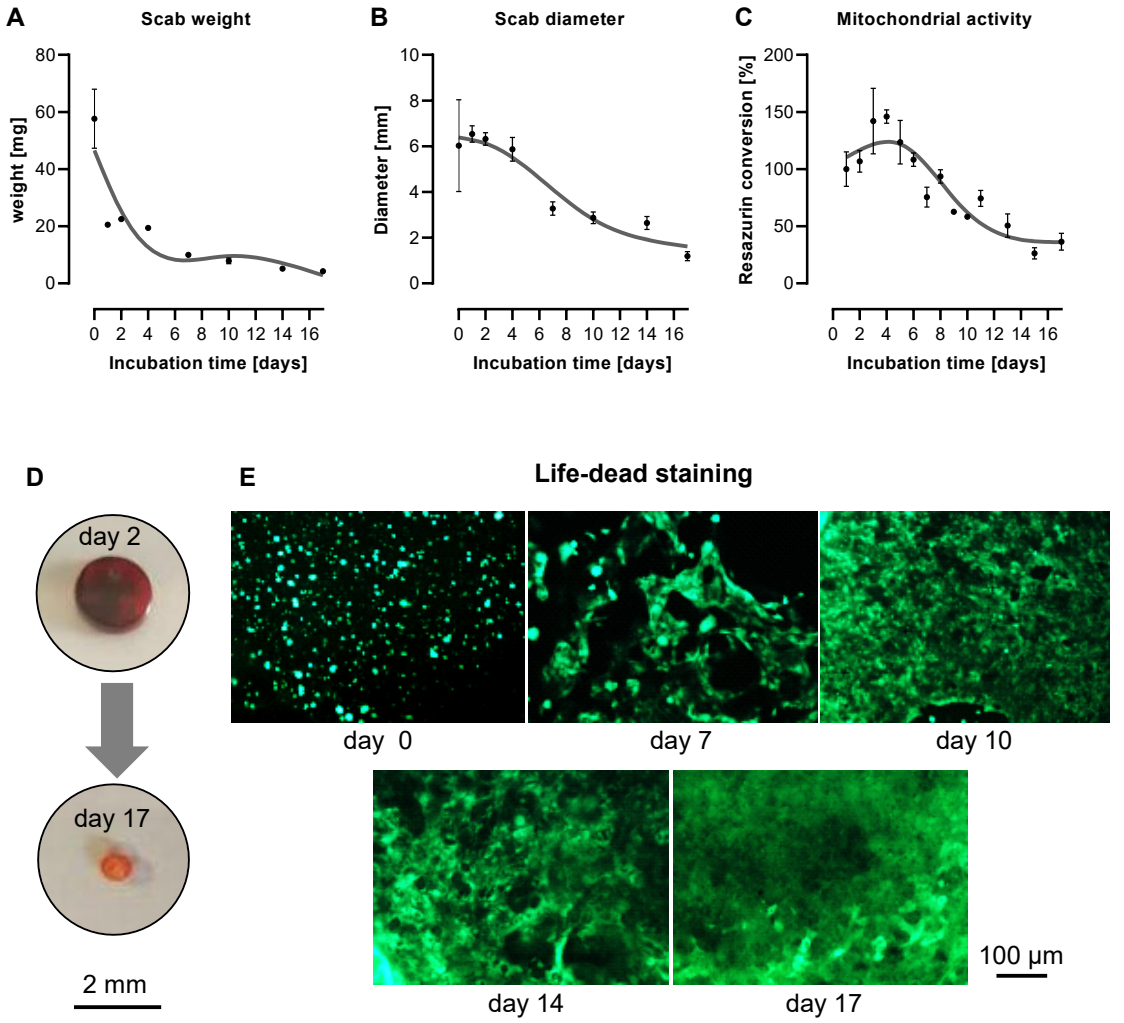

Figure 9: The scab model could be cultured longer than 14 days. (A) Weight of scab in milligrams. N = 4, n≥ 5. (B) Diameter of scab in mm. N = 4, n ≥ 3. (C) The activity of mitochondria is shown as a fold-change from day 0. N = 4, n =3. (D) Scab on day2 and day 17. (E) Staining for viability. A 10-fold magnification was applied to representative images. On days 0, 7, 10, 14, and 17 of culture, pictures were taken.

3.2.2 *Cytokines and chemokines were secreted from the in vitro scabs during the first 7 days.*

The production of cytokines and chemokines during the wound-healing process indicates the involvement of immune cells in this process. Here the immune cells were characterized by the production of chemokines and cytokines. RT-PCR was done to ascertain the production of cytokines and chemokines throughout the first 7 days of incubation (Liu, Rinderknecht et al. 2022). The expression of IL-1α peaked around day 5, then decreased (Figure 10A). IL-1β increased slightly at the beginning and decreased from day 3 on (10B). IL-8 and CCL2 had the same trend as IL-1β (Figure 10C&D). The expression of CCL5 declined with time (Figure 10E). The trend of CCL7 was similar to CCL5 (Figure 10F).

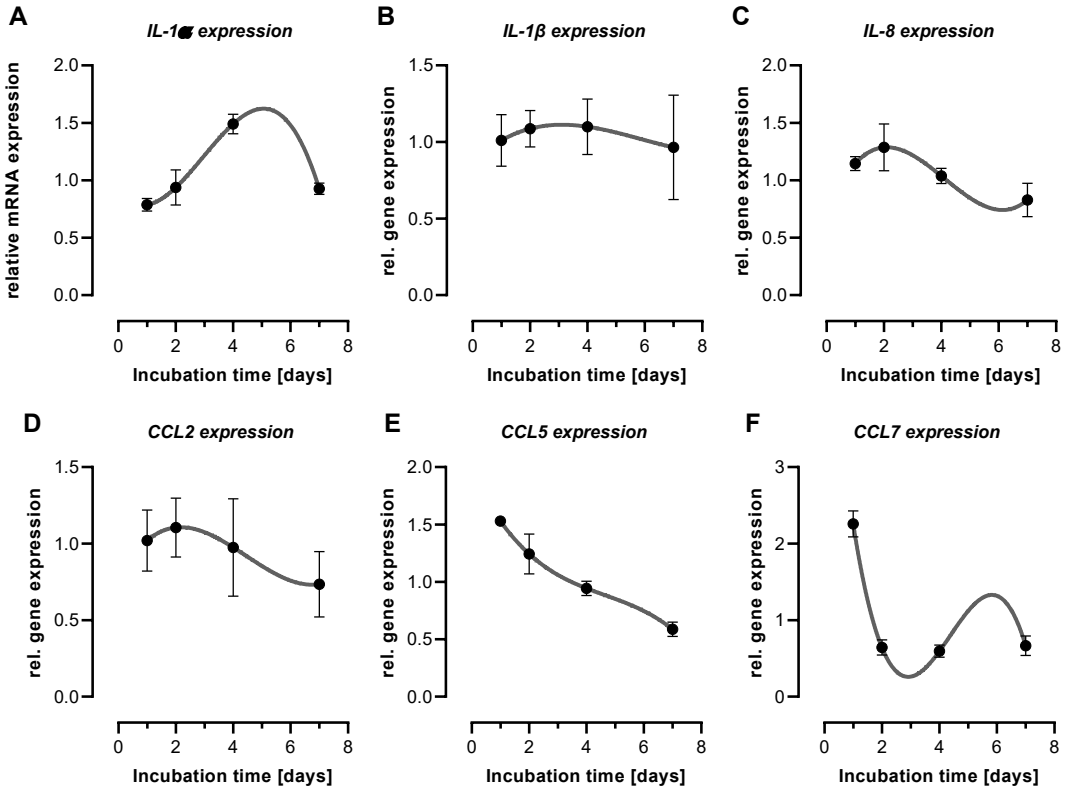

Figure 10: Cytokines and chemokines' expressions in the scab model. RNA was isolated from the scab model and the RT-PCR to check the gene expression. (A) IL-α expression. (B) IL-β expression. (C) IL-8 expression. (D) CCL2 expression. (E) CCL5 expression. (F) CCL7 expression. On days 1, 2, 4, and 7 of culture, expression levels were assessed. N = 4, n = 2.

3.2.3 In vitro scab models expressed TGF-β 1-3.

TGF-β1,2 and 3 expressions were measured using Semi-quantitative RT-PCRs. Within the scab, these three TGF-β isoforms were discovered (Liu, Rinderknecht et al. 2022). The expression of TGF-β1 rose up until around day 5, then decreased; there was an obvious change in the amplitude compared to TGF-β2-3 (Figure 11A). TGF-β2 showed a similar trend as TGF-β1 but with smaller amplitude (Figure 11B). TGF-β3 expression increased at the beginning and started to fall from day 4 (Figure 11C). Besides the gene expression, active TGF-β1 level was measured in the scab supernatant by using an adenoviral-based reporter assay, and the change of active TGF-β1 was similar to the trend of gene expression. Active TGF-β1 rose to the highest level around day 5 and decreased afterward (Figure 11D).

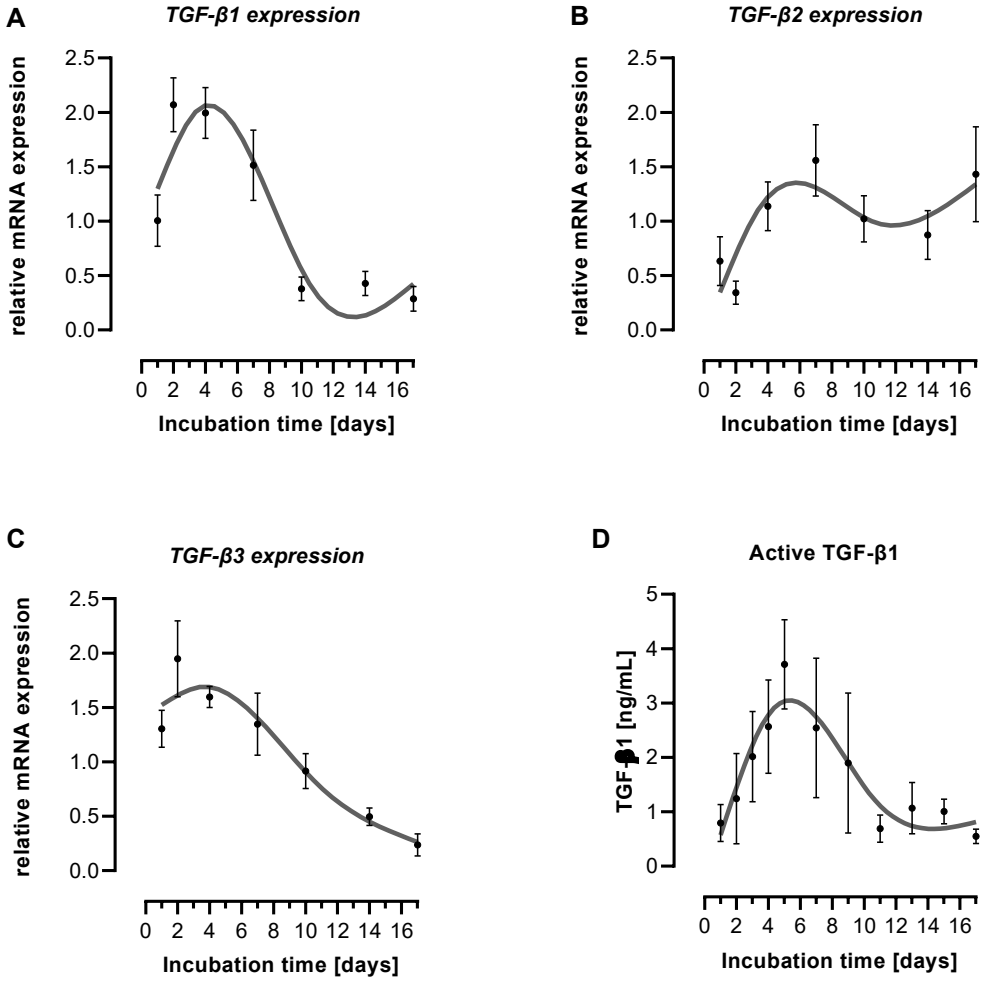

Figure 11: TGF-β expression and secretion over time. (A-C) Gene expression of TGF-β1,2 and 3. The level was determined on the day 1, 2, 4, 7, 10, 14, and 17. N = 4, n = 2. (D) An adenoviral-based reporter assay was applied to identify the active TGF-β in the supernatant of the scab. N = 4, n = 2.

3.2.4 Target genes for TGF-β

TGF-β also played its role through its target genes (Liu, Rinderknecht et al. 2022). As a direct downstream mediator of *TGF-β,* the expression of *CTGF* was similar to the trend of *TGF-β1* (Figure 12A). F*ibronectin (FN1)* expression increased slowly until day 7, then decreased (Figure 12B). Type I collagen

(*CoL1A1*) rose throughout the culture (Figure 12C). In addition, *TGF-β1* can also modulate angiogenesis. Expression of *VEGFA*, which plays potent roles in angiogenesis, increased with time (Figure 12D).

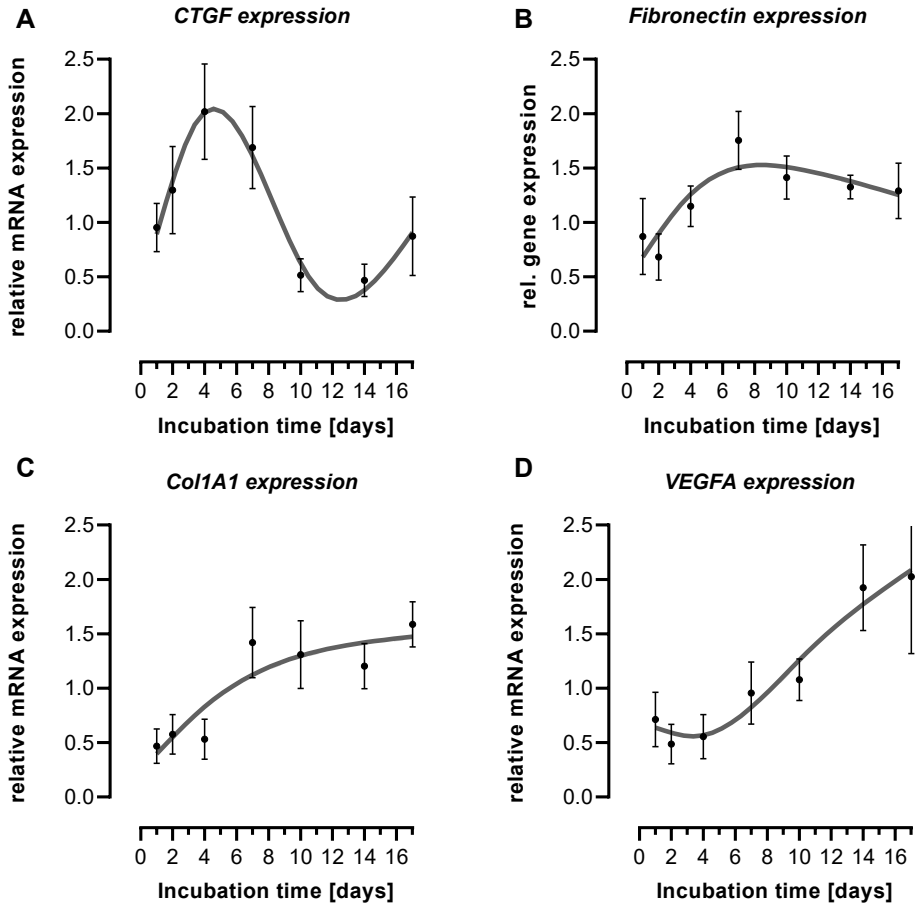

Figure 12: *TGF-β* target gene *expression changes with time*. RNA was isolated from the scab and the RT-PCR to check the gene expression. (A) *CTGF* expression. (B) *Fibronectin* expression. (C) *CoL1A1* expression. (D) *VEGFA* expression. On culture days 1, 2, 4, 7, 10, and 14, expression was assessed. N = 4, n = 2.

3.2.5 MMPs and TIMPs were involved in ECM degradation.

Matrix metalloproteases (*MMPs*) degrade ECM in acute and chronic wounds (Liu, Rinderknecht et al. 2022). *MMP1* expression elevated first, then declined

from day 7 on (Figure 13A). The expressions of *MMP2*, *MMP9*, and *MMP13* showed similar patterns with the highest levels observed at around day 7 of culture (Figure 13B, C, D). As the main inhibitors of MMPs in the wound, *TIMP1* and *2* were also detected in the scab. After approximately two weeks of culture, the expression of *TIMP1* and *TIMP2* rose and plateaued (Figure 13E, F).

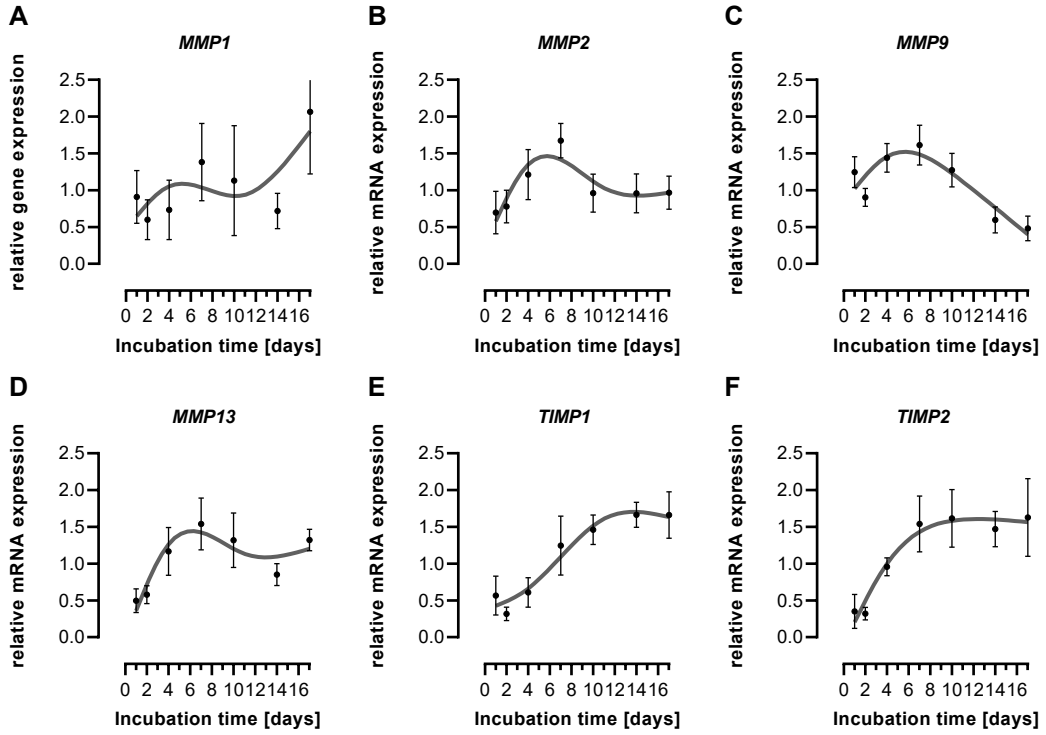

Figure 13: *MMPs* and *TIMPs* expression in the scab over time. RNA was isolated from the scab model and RT-PCR was used to check the gene expression. (A-D) *MMP1, 2, 9, 13* (E-F) *TIMP1*, *2*. Timepoints were on days 1, 2, 4, 7, 10, and 14. N = 4, n = 2.

3.2.6 Active MMP9 was detected in the supernatant of the scab.

Gelatin zymography was carried out to check for MMP9 activity in the supernatant of the *in vitro* scabs (Figure 14A). It showed the same trend with MMP9 gene expression in the *in vitro* scabs. Functional MMP9 level went up from the beginning, then dropped/decreased after 5-6 days (Figure 14B).

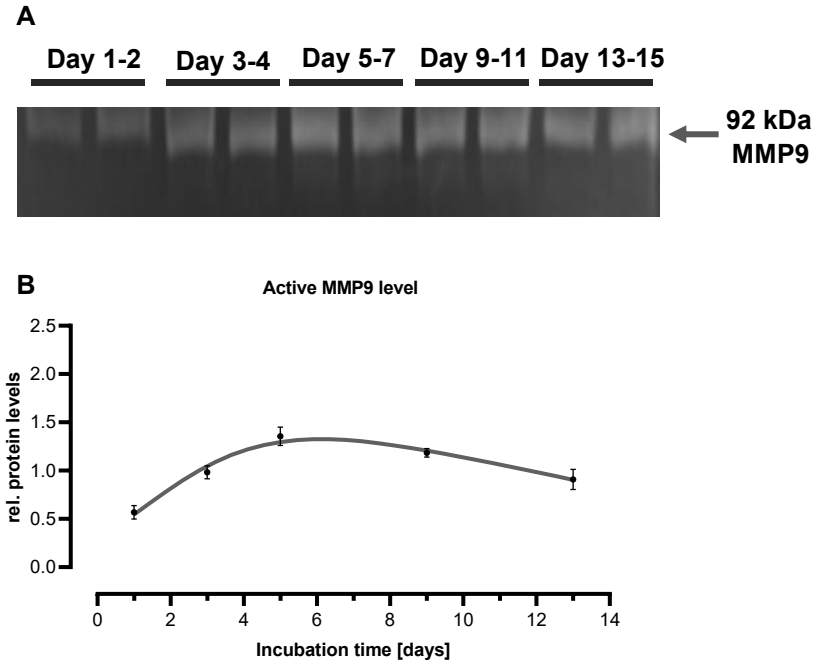

Figure 14: Activity MMP9 in the supernatant of the in vitro scab by gelatin Zymography. The supernatant was collected and made a pool separately at different time points. (A) Representative bands on gels. Gelatin zymogram banding patterns are demonstrated for the 5 supernatant samples pooling on different time points. (B) Quantitative data of the active level of MMP9. The supernatant obtained on days 1, 2, 3, 4, 5, 7, 9, 11, 13, and 15 of culture, and mix the supernatants every two days in a pool. N = 4, n = 2.

3.2.7 Amounts of growth factors were released from this scab model.

In addition to TGF-β, relative levels of various growth factors in the supernatants were determined using human growth factor array 5 (ray bio), following the manufacturer's instructions. Overall, signals for EGF (Epidermal growth factor) and SCF (supercoiling factor) receptors were strongest. While EGFR decreased with time, SCFR increased with time. On the contrary, signal intensities for VEGFR2, bNGF (neurotrophic factor nerve growth factor), PDGFRa (platelet-derived growth factor receptor alpha), IGFBP (insulin-like growth factor binding protein) -3, and -6 were nearly to or even below the limit of detection (Figure 15A). The three TGF-β isoform levels matched the results of

the gene expression study. Levels of M-CSF (Macrophage colony-stimulating factor 1), G-CSF (granulocyte colony-stimulating factor), and IGF-II (insulin-like growth factor II) increased with time. Inversely, EGF (epidermal growth factor) levels and IGFBP-1 and -4 decreased with time. Levels of SCF and soluble receptors of IGF-I peeked early within the observation frame (Figure 15A). To better display changes in the growth factor levels over time, the array data were normalized to the first-time frame (day 1+2). (Figure 15B) This analysis revealed that TGF-β1 and IGF-II showed the most robust increase (8- to 9-fold) over time in the *in vitro* scabs. Followed by SCF receptor, M-CSF, GM-CSF (granulocyte-macrophage colony-stimulating factor), and G-CSF, which showed a 4- to 5-fold increase over time. Inversely, the most substantial decline was observed for EGF and IGFBP-4, followed by HGF (hepatocyte growth factor) and AR (androgen receptor).

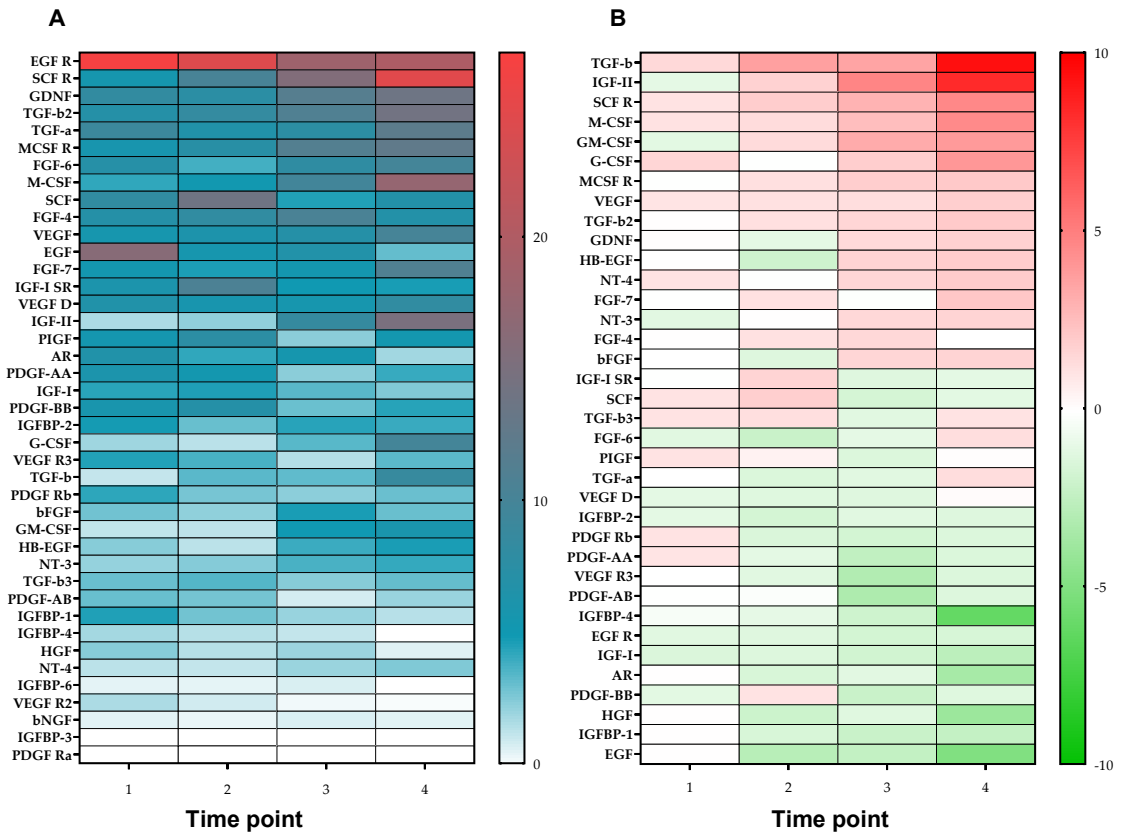

Figure 15: Heat map from the human growth factor Array. Culture supernatants from 4 donors (N = 4) were pooled to cover the time frames between days 1-2 (time point 1), 3-4 (time point 2), 5-7 (time point 3), and 8-10 (time point 4). The growth factor array was performed twice (n = 2). All targets were spotted in duplicates. The luminescent signal was developed with ChemoCam (INTAS). Quantification of intensity was determined by the ImageJ software and normalized to the positive controls spotted on the array. The GraphPad Prism software generated a heat map showing the relative growth factor levels (positive control = 100%). (A) Secreted growth factors are listed from the lowest (white) to the highest (red) level. (B) The increased (red color) and decreased (green color) growth factors with the culture time.

3.3 Exogenous TGF-β1 played a prominent role in the scab model.

3.3.1 Determination of exogenous TGF-β isoform concentration

This scab model was characterized by the changes of TGF-β1-3 and its related target genes. To confirm the effect of TGF-β1-3, exogeneous TGF-β1-3 and its inhibitor Alk5i were administered on this scab model *in vitro* separately (Liu,

Rinderknecht et al. 2022). The concentration of exogenous TGF-β1-3 and Alk5i was determined by Smad2/3 reporter assay. The physiological TGF-β levels were also taken into consideration at the same time. Hence, 10 ng/mL, 5 ng/mL, and 1 ng/mL were the concentration of exogenous TGF-β1-3 respectively. The concentration of Alk5i was 500 nM, which could inhibit these three TGF-β isoforms (Figure 16 A-C).

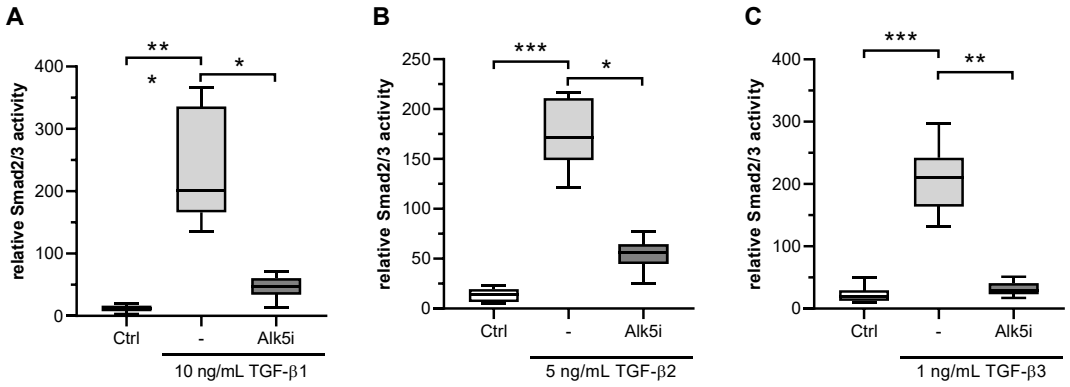

Figure 16: Inhibition of TGF-β isoforms on Smad2/3 activity. The exogenous activation of TGF-β signaling was examined by using an adenovirus-based reporter assay. TGF-β1-3 signaling was successfully inhibited by 500 nM Alk5i (SB431542). (A) TGF-β1 10 ng/mL, (B) TGF-β2 5 ng/mL, and (C) TGF-β3 1 ng/mL dramatically increased TGF-β signaling in scab. The data were compared using the Kruskal-Wallis test multiple comparisons. *** p = 0.001, ** p = 0.05, and * * * * p = 0.05.

3.3.2 Exogenous TGF-β1 maintained the stability of the scab.

Exogeneous TGF-β1-3 or Alk5i were added to the scabs every second day for a total of 14 days. At the end of days 2, 7, and 14 of culture, the scabs were examined. Weight, area, and mitochondrial activity in the scab were measured to assess the scab models' stability. On the first time point, day 2, the groups differed from one another. On the second time point, day 7, the differences in scab weight, diameter, and mitochondrial activity between TGF-β1 and Alk5i groups started to appear (Figure 17 A-C), and it became more evident on day 14.

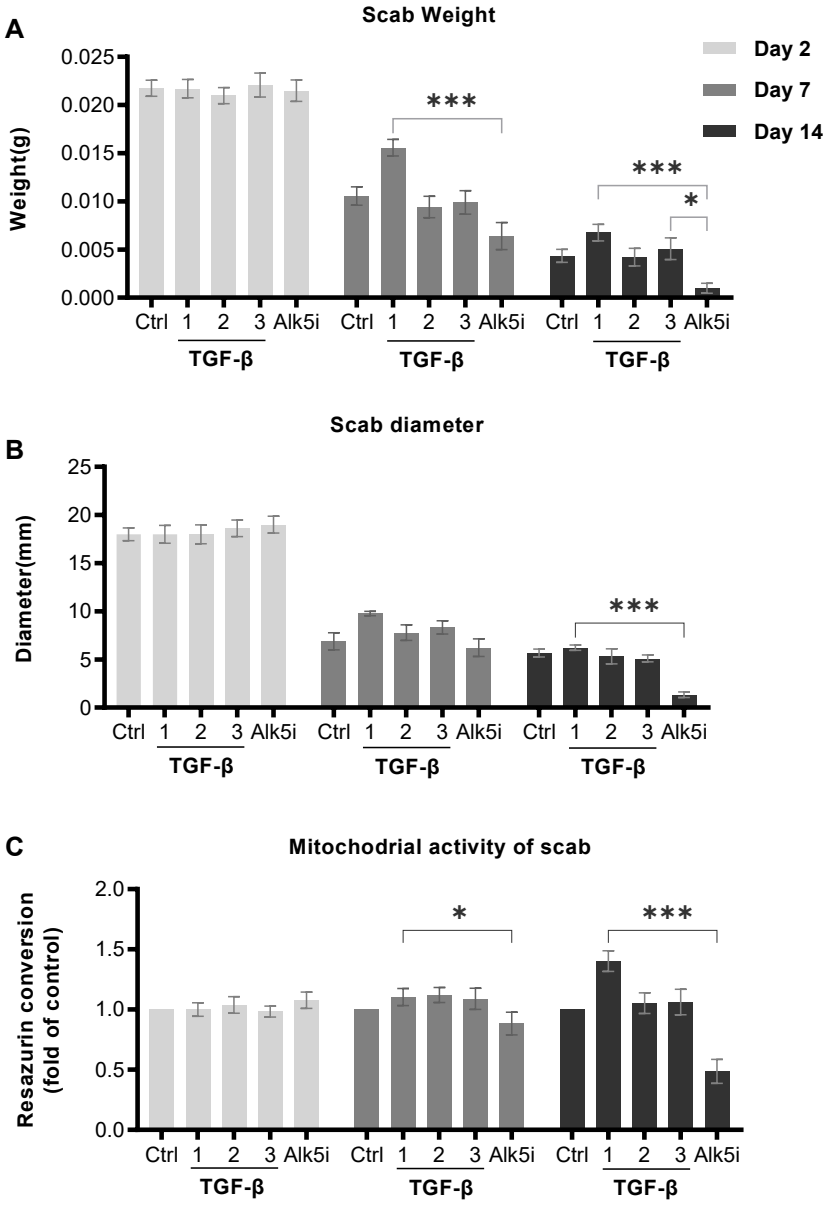

Figure 17: Changes of scab on weight, area, and mitochondrial activity with exogenous TGF-β1-3 and Alk5i. (A) Scab weight. (B) Scab diameter. (C) Mitochondrial activity fold of control from day 2 was displayed. N= 4, n =3. As box plots, data were displayed. The data was compared using a 2-way ANOVA. *** p = 0.001, ** p = 0.05, and * * * * p = 0.05.

After 14 days of incubation, obvious differences were observed among the 5 groups (Liu, Rinderknecht et al. 2022). *In vitro*, the group with alk5i scabs had

the lightest weight, smallest area, and lowest mitochondrial activity. In contrast, scabs stimulated with TGF-β1 obtained maximum weight, volume, and mitochondrial activity. Scab volume, weight, or mitochondrial activity were not significantly affected by exogenous TGF-β2 or TGF-β3 stimulation (Figure 18 A-C). Judging from the appearance, scabs in the Alk5i group were the smallest size and the palest in color (Figure 18 D).

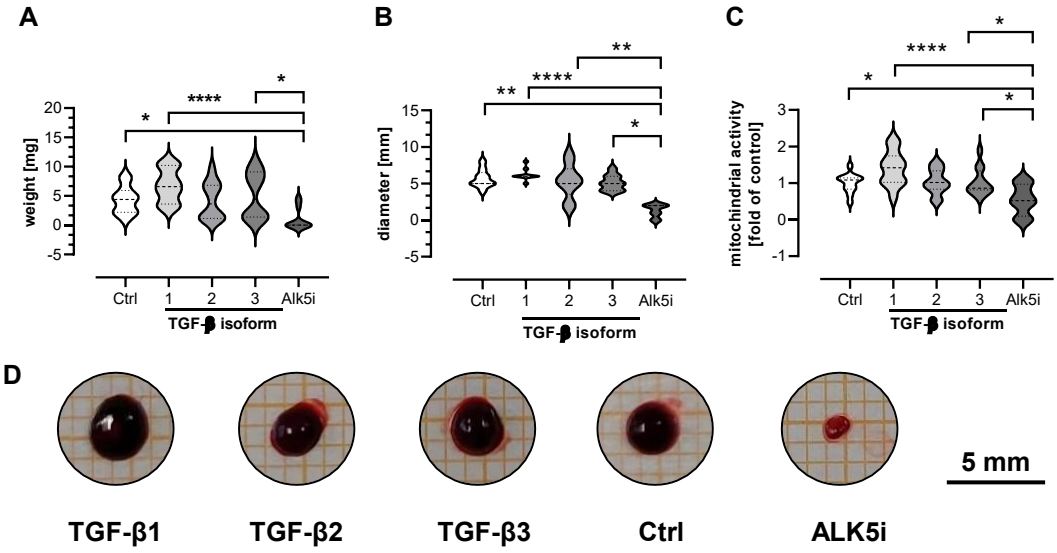

Figure 18: Exogenous TGF-β1-3 and Alk5i produced significant differences in the weight, area, and mitochondrial activity of scabs on day 14. Exogenous TGF-β1-3 and Alk5i were added to the in vitro scab for 14 days. (A) Weight. (B) Area. (C) The activity of the mitochondrial. N = 4, n =3. (D) The pictures are on the 14th day of culture. The data were contrasted using a non-parametric one-way ANOVA and then displayed using box plots, along with Dunn's multiple comparison test. * p = 0.05, ** p = 0.01, *** p = 0.001, and **** p = 0.0001 as compared to Alk5i group.

3.3.3 Exogenous TGF-β1 leads to upregulation of Smad7 in the scab.

Semi-quantitative RT-PCR was conducted to examine *TGF-β* target genes expression in the scabs of *in vitro (Liu, Rinderknecht et al. 2022)*. The result showed that exogenous TGF-β1 promoted the production of *Col1A1*, *FN1,* and *CTGF* (Figure 19A-C). Exogenous TGF-β2 and TGF-β3 had a less noticeable

effect. Exogenous TGF-β1 stimulation also increased the expression of its inhibitor *Smad7*, which could inhibit the TGF-β signal pathway (Figure 19H). *MMP9* expression was promoted by TGF-β1-3 and Alk5i (Figure 19D). The stimulation had no appreciable impact on *TIMP1* or *TIMP2* expression (Figure 19E-F). The ratio of *MMP9/TIMP1* which represented the matrix breakdown was increased with exogenous TGF- β1(Figure 19G).

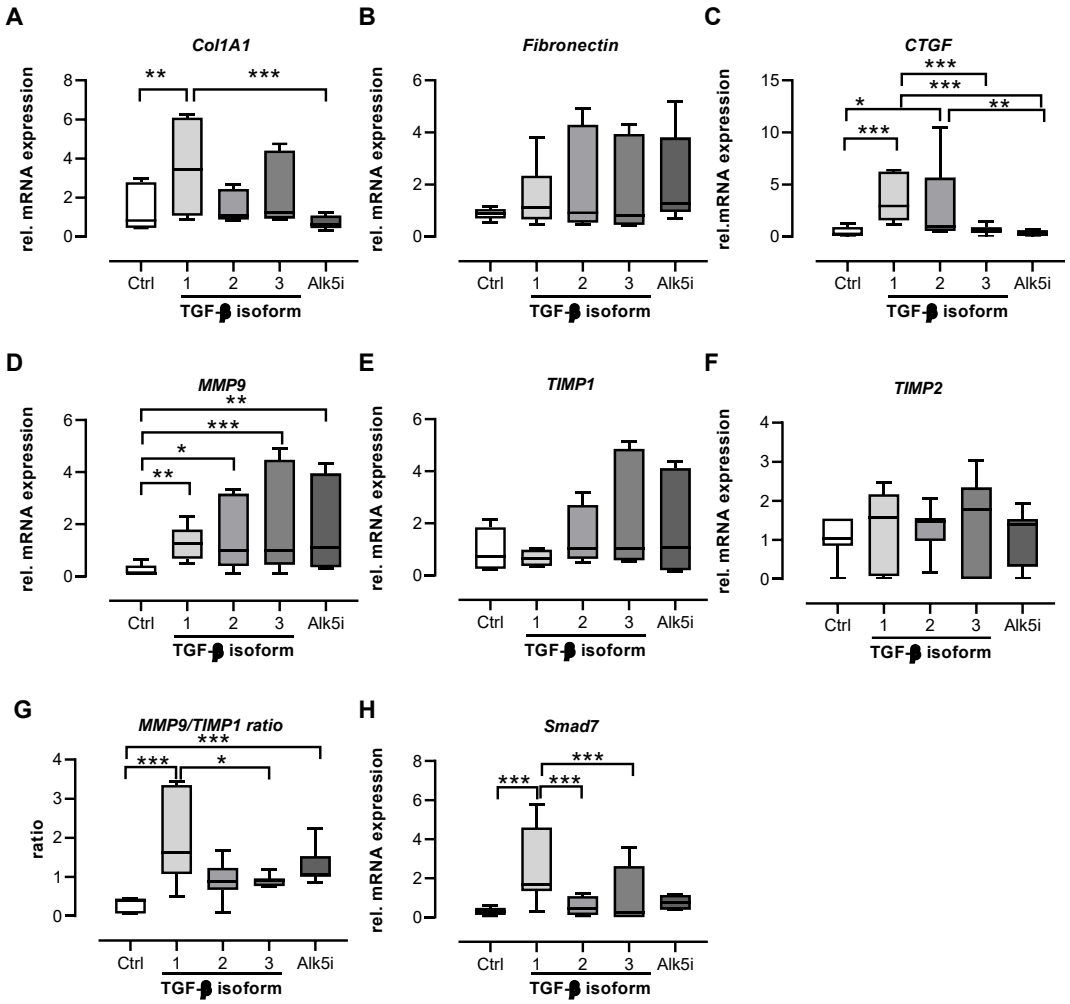

Figure 19: ECM-related gene expression in scab. After 14 days of culture, gene expression was analyzed, compared to the levels of the housekeeping genes, and shown.: (A) *CTGF*, (B) *Col1A1*, (C) *FN1*, (D) *MMP9*, (E, F) *TIMP1* and *TIMP2* (G) the MMP9 to *TIMP1* ratio, (H) *Smad7*. N = 4, n = 3. Box plots were used to display the data. Dunn's multiple comparison tests and

non-parametric one-way ANOVA were conducted to compare the data. * p = 0.05, ** p = 0.01, *** p = 0.001, and **** p = 0.0001 contrastingly with Alk5i group.

3.3.4 Recombinant human TGF-β1 promotes angiogenesis in the scab model.

As a versatile growth factor, TGF-β1 has been reported to promote angiogenesis *in vivo* and *in vitro* (Vinals and Pouyssegur 2001). After adding exogenous TGF-β1-3 and Alk5i to *in vitro* scabs, the angiogenesis in the *in vitro* scabs was evaluated by different experimental methods.

3.3.4.1 TGF-β1 increased the junctions and mesh area.

In the tube formation assay, the tube formation represented the angiogenesis ability of the supernatant. The supernatant from the TGF-β1 group started to produce tubes earlier than other groups, and more tubes were formed with time (Figure 20A) (Ehnert, Rinderknecht et al. 2023). In TGF-β2 and 3 groups, the tubes began to be produced until time point 2 (day 5-6) (Figure 20A). Then, time point 3 (days 12-14) was chosen to check the differences among groups. To compare with the supernatants, the same amount of exogenous TGF-β1-3 and Alk5i were added to the culture medium. Junctions and mesh area were used to evaluate the tube formation. The result showed that supernatant from the TGF-β1-3 group produced more junctions and mesh area (Figure 20B&C).

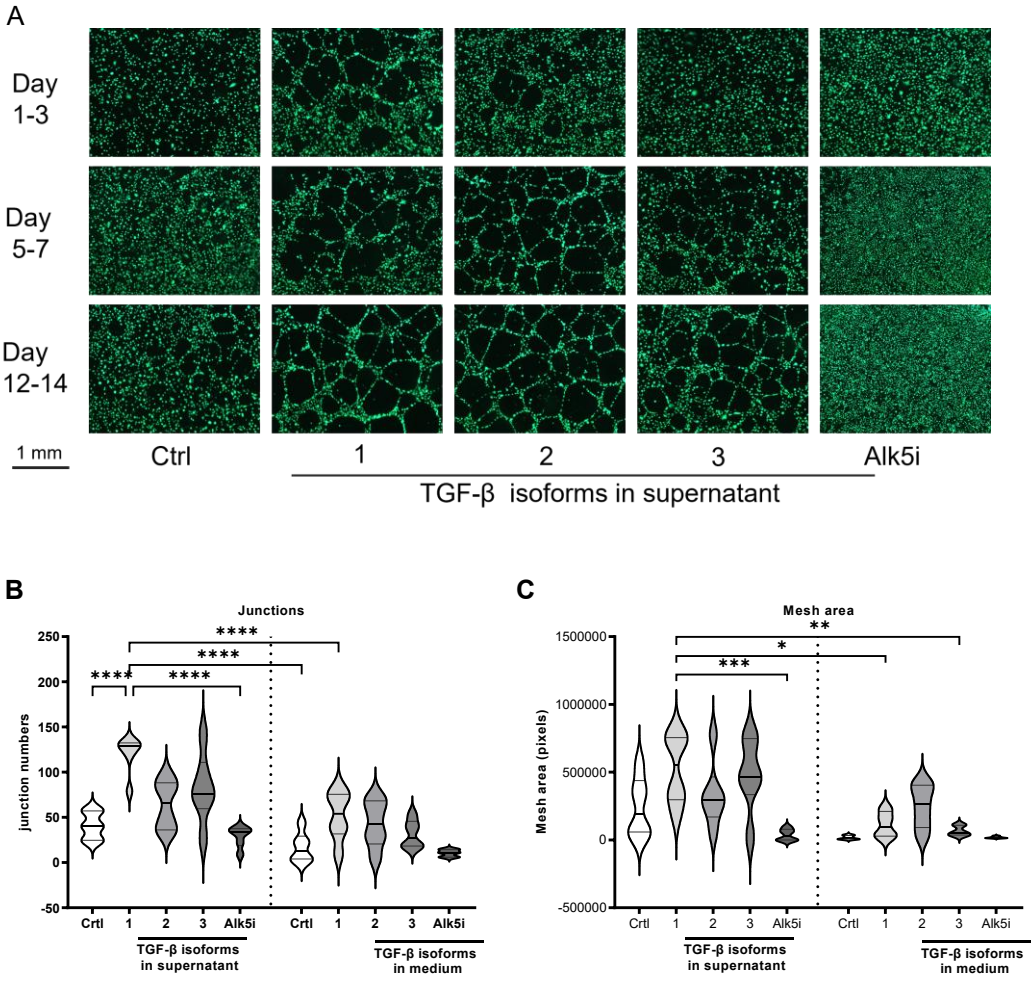

Figure 20: HUVEC Tube formation assay measured by junctions and mesh area. (A) Representative images of the tubular structures formed after adding the supernatant on different time points were taken with a 4X object lens (scale bar = 1 mm). (B-C) Junction numbers and mesh area formed with supernatants on days 12-14 and medium with TGF-β1-3 or Alk5i. N = 2, n = 3. The data was compared with non-parametric one-way ANOVA multiple comparison tests. * p = 0.05, ** p = 0.01, *** p = 0.001, and **** p = 0.0001.

3.3.4.2 Exogeneous TGF-β1 promoted the production of angiogenic factors.

Angiogenesis array C2 was applied to investigate the angiogenic factors in the supernatant of culture. The supernatant pools were prepared as described before, and only the supernatants of timepoint 3 were checked. In the TGF-β1 and 3 groups, more angiogenic factors were produced, and the least angiogenic

factors were produced in the inhibitor group (Figure 21A). The constellation plot showed that two groups of angiogenic factors (with a red circle) were upregulated by the supernatant from the TGF-β1 group and downregulated by the supernatant from the Alk5i group, including the factors Angiopoietin-1, Angiopoietin-2, VEGFR3, IL-2, IL-4, IL-10, Endostatin, and GM-CSF (Figure 21B) (Ehnert, Rinderknecht et al. 2023).

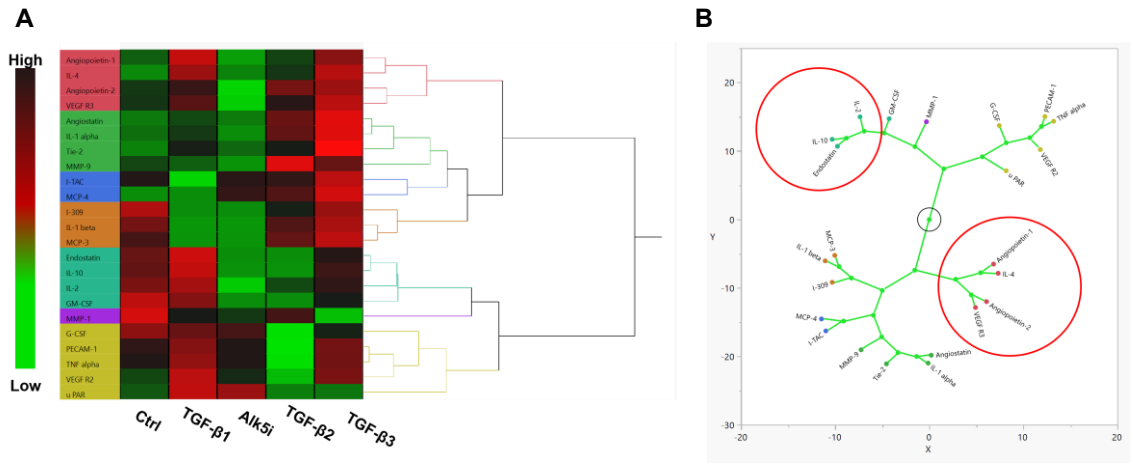

Figure 21: Angiogenic gene expression with different supernatant. (A) Angiogenesis factors produced in supernatants on time point 3 (days 12-14) were displayed in a heat map. (B) Constellation plot: Angiogenesis factors in TGF-β1 and Alk5i groups had the same or opposite effect and formed different clusters. N = 2, n = 3.

3.3.4.3 The expression of VEGFA was upregulated by exogenous TGF-β1.

As the most important angiogenic factor, the gene expression of VEGFA was checked after adding the TGF-β isoforms or Alk5i. On day 2 and day 7, no differences were found among the groups (Figure 22A-B). On day 14, VEGFA levels in the TGF-β1 group were the highest (Figure 22C) (Ehnert, Rinderknecht et al. 2023).

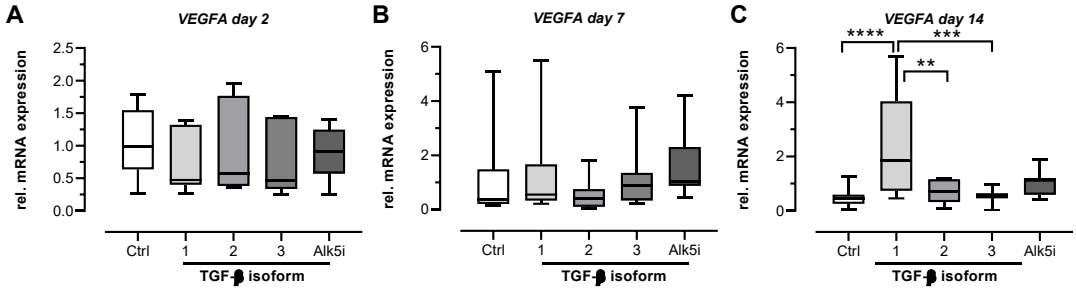

Figure 22: *VEGFA* expression after adding TGF-β1-3 or the inhibitor (Alk5i). RNA was isolated from the in vitro scab, and RT-PCR was done to check the gene expression. (A) VEGFA gene expression on day 2. (B) VEGFA gene expression on day 7. (C) VEGFA gene expression on day 14. N = 4, n = 3. Box plots are used to display the data. Wallis test and non-parametric one-way ANOVA were applied to analyze the data. * p = 0.05, ** p = 0.01, *** p = 0.001, and **** p = 0.0001 as compared to TGF-β1 group.

4. Discussion

In recent years, chronic wounds attracted increasing attention because of rising morbidity, long-term duration (at least more than 30 days), high disability rate, and high cost of treatment (Falanga, Isseroff et al. 2022). Exploring the mechanisms behind chronic wounds is critical for new treatment development. Wound healing is achieved under the coordinated action of various growth factors. Although the importance of TGF-β1-3 isoforms has been verified in normal wound healing, we found higher TGF-β1 expression in samples of patients with chronic wounds, but the increase of TGF-β1 didn't improve the wound healing like in acute wounds. Exploring this discrepancy will help find possible therapeutic targets.

4.1 Overexpressed TGF-β1 in chronic wounds

Among many different growth factors, TGF-β is of the most interest considering its involvement in the whole process of wound healing. TGF-β1-3 exerts different functions in the healing process, TGF-β1 is critical for extracellular matrix formation, angiogenesis, and regulation of inflammation in wound healing. Moreover, TGF-β1 can also improve keratinocyte migration (Gailit, Welch et al. 1994). It is noteworthy that TGF- β1 expression is increased in scar tissue, promoting the proliferation of fibroblasts, as well as the cell differentiation and production of collagen (Liu, Li et al. 2016).

However, the results from patients showed overexpressed TGF-β1 in chronic wound tissue. This means that the increased TGF-β1 in chronic wounds didn't function in its role as in normal wound healing. TGF-β1-3 is produced in a latent state, which can be switched on by low PH, ROS, proteases, and shear forces (Taylor 2009). The active TGF-β performs its function by the TGF-β signaling pathway. With serum samples from the same patients, active TGF-β levels were

investigated by a luciferase reporter assay. At the same time, we found that TGF-β1 expression increased with culture time.

Additionally, TGF-β is also context-dependent (Morikawa, Derynck et al. 2016). The samples included most of the wound types, although the central part was traumatic wounds. The distribution of wound types in the two groups was also similar. Primarily overexpressed TGF-β1 was one of the characteristics of chronic wounds. The most exciting point is that the overexpressed TGF-β1 also differed from the increased TGF-β1 in keloid tissue, where TGF-β1 can produce more scar tissue than the non-healing wound (Lichtman, Otero-Vinas et al. 2016). Therefore, it was proposed that even though it was active, TGF-β1 in chronic wounds did not function normally. So, we needed to detect mechanisms leading to overexpressed TGF-β1 in chronic wounds.

The TGF-β2 function is similar to TGF-β1 and related to granular tissue formation and angiogenesis (Barrientos, Stojadinovic et al. 2008). Compared with TGF-β1-2, TGF-β3 inhibits scar formation in wound healing (Schrementi, Ferreira et al. 2008). Our result showed no discernible difference on *TGF-β2* and *TGF-β3* gene expression between acute and chronic wounds. Characteristics of the *in vitro* wound model.

An ideal wound model will not only be the basis of the entire study but also be helpful to test and verify possible therapeutic targets. Although animal models are prevalent, it is constrained by the type of skin, long production processes, hefty cost, and ethical considerations (Hartung 2008). As the wound healing process is directly related to the interplay between blood and skin cells, the model should be able to present this reaction. Here, a co-culture of HaCaT cells and fresh blood was established to represent this interaction (Liu, Rinderknecht et al. 2022).

The established *in vitro* wound model combined HaCaT cells with fresh EDTA blood and $CaCl_2$. $CaCl_2$ was added, which saturated the EDTA and allowed for coagulation (Shida, Kurasawa et al. 2016), simulating the formation of a hematoma or scab. The scabs' weight and area decreased throughout the culture, and the number of HaCaT cells increased, indicating the resorbing and remodeling of scabs *in vivo* (Landen, Li et al. 2016). The decline of blood cells during the co-culture time was anticipated. Gene expression of cytokines supported this hypothesis. The typical cytokines, like *IL-1α*, *IL-1β*, *IL-8,* and *CCL2* were mostly released until day 5 and declined with culture time. For *CCL5* and *CCL7*, the gene expression level decreased continuously.

TGF-β is rapidly secreted by blood cells and keratinocytes, particularly thrombocytes in normal wound healing. The released TGF-β subsequently favors/supports migration, differentiation, proliferation, and ECM synthesis of keratinocytes (Pakyari, Farrokhi et al. 2013). The here-presented *in vitro* scabs also secreted active TGF-β, notably in the first days of culture. Similarities existed in *TGF-β1-3* expression and the production of active TGF-β1. This outcome aligns with previous research results, which showed a significant rise in activated TGF-β1 levels early during wound healing (Yang, Qiu et al. 1999).
Additionally, TGF-β can produce different effects indirectly by its target genes. One of the important functions of TGF-β is to control ECM formation in wound healing (Hyytiäinen, Penttinen et al. 2004). Besides providing structural support for the tissue during wound healing, the ECM also regulates how cells attach, migrate, proliferate, and differentiate (Roberts, Mccune et al. 1992). *TGF-β1* target genes, such as *CTGF*, *Col1A1*, and *FN1*, are involved in synthesizing the ECM (Tracy, Minasian et al. 2016). The studies of *in vitro* presented that non-classical TGF-β signaling causes CTGF production (Secker, Shortt et al. 2008). In our scab model, *CTGF* expression, similar to *TGF-β1*, was upregulated until

day 5-6 of culture. This early increase in CTGF expression might explain the increased expression of *Col1A1* and *FN1* in developing granulation tissue in wounds (Frazier, Williams et al. 1996). It was reported that *Col1A1* and *FN1* could be increased by TGF-β in different cell types (Ignotz and Massague 1986, Roberts, Heine et al. 1990). Hence, it is unsurprising that the expression of *Col1A1* and *FN1* increased in our scab model. In the early period of wound healing, collagen III is first to be produced; collagen I eventually takes its place (Mathew-Steiner, Roy et al. 2021). *VEGFA* expression in *in vitro* scab increased with time, which was consistent with its expression in the process of normal wound healing. TGF-β induced angiogenesis by an immediate and temporary apoptotic effect on endothelial cells mediated by VEGFA (Ferrari, Cook et al. 2009). In wound healing, ECM degradation and formation work dynamically together to restructure the tissue architecture (Lu, Takai et al. 2011). *MMP1, 2, 9,* and *13* and the inhibitors *TIMP1* and*, 2* were detected in our scab model. The expression of these four *MMPs* increased during the first 5-7 days of culture, and *TIMP1-2* was with a similar trend; which may indicate the synergy between MMPs and TIMPs. Similarly, the expression of *MMPs* and *TIMPs* can also be regulated by *TGF-β (Krstic and Santibanez 2014)*. Here, the reason for the high basal expression of *MMP9* may be that keratinocytes can express *MMP9* in the wound. In delayed wound healing, *MMP-9* expression is dysregulated and overexpressed (Reiss, Han et al. 2010). With Gelatin zymography, active MMP9 has checked the same trend as the gene expression in this *in vitro* scab. At the same time, amounts of other growth factors were also detected in the supernatant of this *in vitro* scab by Growth factor array, and these growth factors changed with time and different trends.

In summary, this *in vitro* scab model involved two main cell types of skin, blood cells and epithelial cells, and the interaction between blood cells and epithelial

cells was shown by the change of different growth factors and cytokines, which was similar to normal wound healing.

4.2 The impact of exogenous TGF-β1-3 and Alk5i on the scab model

To further verify the function of TGF-β1-3 in these scabs, exogenous TGF-β1-3 and its inhibitor Alk5i were applied separately. Scab stability, viability, *TGF-β* target gene expression, and angiogenesis were used to check the changes in this *in vitro* scab. Exogeneous TGF-β1 maintained the scab for a longer time, and its inhibitor Alk5i had an adverse effect. This phenomenon could partly be explained that ECM formation was increased by the upregulation of *Col1A1.* It can also be explained from the perspective of ECM remodeling. *MMP-TIMP* complexes are formed in a 1:1 ratio in the human body (Cabral-Pacheco, Garza-Veloz et al. 2020), and the ratio of *MMP9/TIMP1* was suggested to be useful in predicting impaired wound healing (Ladwig, Robson et al. 2002). Additional TGF-β1 increased CTGF expression which could also promote ECM formation in the scab. *Smad7*, as the endogenous inhibitor of TGF-β, was checked in the scab. Increased *Smad7* expression indicated the emergence of an auto-regulatory mechanism with exogenous TGF-β1 (Nakao, Afrakhte et al. 1997). This self-inhibitory mechanism also limited the function of TGF-β1 in the scab. Since hypertrophic scar development is caused by increased TGF-β1 activation in wounds (Zhang, Wang et al. 2020), these findings might alter when fibroblasts are added to this scab model.

Wound healing is accomplished through neovascularization. The delivery of oxygen, nutrients, and growth factors depends on the reconstruction of new blood vessels. Poor blood supply is a feature of most chronic wounds. TGF-β is a crucial regulator of angiogenesis and stimulates the production of VEGF which works as a central role of angiogenesis (Brunner and Blakytny 2004,

Verrecchia and Mauviel 2007, Paola and Joseph 2017). In particular, vascular endothelial cells are subject to numerous actions of TGF-β1 (Ferrari, Cook et al. 2009). So, the angiogenic ability of exogenous TGF-β in the scabs needed to be identified. In the Tube formation assay, TGF-β1-3 could improve angiogenesis, especially TGF-β1, which could initiate angiogenic effects earlier and more significantly than TGF-β2 and TGF-β3. Exogenous TGF-β1-3 in the medium also produced more angiogenic factors, which was less evident than the supernatant. It means that TGF-β directly promotes angiogenesis and may indirectly increase angiogenesis by producing more angiogenic factors by the scabs. Angiogenic factors were identified with an angiogenesis array. More angiogenic factors were released into the supernatant supplemented with exogenous TGF-β. With the cluster analysis of software JMP, two groups of angiogenetic factors were detected with the same trend, which was increased with TGF-β1 and inhibited with Alk5i. One group included angiopoietin-1/2, IL-4, and VEGFR3, another group was with endostatin, IL-10, IL-2, and GM-SCF. IL-4 and endostatin produce a negative effect on angiogenesis by inhibiting endothelial cells (Volpert, Fong et al. 1998, Shichiri and Hirata 2001), but the other 6 growth factors can promote angiogenesis. Meanwhile, the predominant angiogenic factor VEGFA was also checked in the in vitro scabs. After adding TGF-β1, VEGFA expression was significantly increased on the 14th day.

In conclusion, this scab model could be cultured for more than two weeks, including the initial stages of typical wound healing process. It released and expressed TGF-β1-3 and their target genes following expectations for regular wound healing. Characteristic alterations in *in vitro* scab that were connected to impaired wound healing have been seen by altering TGF-β signaling. As a result, this scab model can be utilized to check the mechanisms in *in vitro* on the stages of early wound healing.

4.3 Chronic trauma wounds were with impaired TGF-β signaling pathways.

High TGF-β1 levels were discovered in wound tissue and plasma from patients with chronic wounds. This conflicted with the result in the literature, and more TGF-β1, even activated TGF-β1, could not be beneficial to chronic wounds. With the scab model, it was also verified exogenous TGF-β1 positively affected proliferation, ECM formation, and angiogenesis. So, the possibility might be the impaired TGF-β signaling pathway.

The TGF-β signal via Smad2/3, and Smad3 is necessary for a variety of cell responses to damage (Roberts, Russo et al. 2003). Once this pathway is activated, Smad2/3 is phosphorylated(Yuan, Ren et al. 2022). So, phospho-Smad3 was chosen as the target protein to check the TGF-β signal pathway. Since traumatic wounds were the main parts of the patient's samples, traumatic wounds were the research objects to make the two groups comparable. With Western blot, the levels of phospho-Smad3 were investigated (Mu, Zuo et al. 2019). A low level of phospho-Smad3 was found in chronic wound tissue samples. This significant difference proved the idea of impaired TGF-β signaling pathway in traumatic chronic wounds (Ramirez, Patel et al. 2014).

After identifying the impaired TGF-β signaling pathway, the best strategy was to find the location of an impaired signaling pathway in cells (Gifford, Tang et al. 2021). Immunohistochemistry staining was done, and the result showed reduced phosphorylation of Smad3 in the nucleus in chronic wounds tissue compared to acute wounds. Although there was no statistical significance, the trend was still obvious. Considering the limitation of sample amounts, there were only 15 samples in total, in the future more samples are needed to improve the result. Of course, in the process of manual counting, there will inevitably be human factors affecting the results. It also needs to consider how to improve to make the results more objective.

Since TGF-β impaired signaling pathway was identified in chronic wounds, the causes of the impaired signaling pathway await further study. The most likely of these is the presence of inhibitory factors. The inhibitors could function as a negative feedback loop by preventing the phosphorylation or nuclear translocation of receptor-associated Smads (PIEK, HELDIN et al. 1999, Massagué 2000). There are two kinds of inhibitors. One is related to the TGFβ receptor, like BAMBI (Fan, Li et al. 2015) (Ehnert, Rinderknecht et al. 2023), and another type plays its role by inhibiting phosphorylation of Smad2/3 or interfering with the formation of the Smad2/3-Smad4 complex, like Smad 7, SARA, or Smurf (Halder, Beauchamp et al. 2005). Identifying the right inhibitors will provide more effective and reliable targets for future treatments.

4.4 Study limitations.

In this study, there were still some limitations. As far as this model is concerned, although it is a co-cultured 3D model of blood cells and HaCaT cells, another major cell type in the skin, fibroblasts, is still missing. Therefore, it does not fully reflect the real skin wound. How to achieve co-culture with fibroblasts is the key to perfecting the in vitro model.

Regarding the patients' samples, the sample size in our study was limited. There were only 37 samples of patients in total, and in the immunohistochemistry staining, there were not more than 10 slide sections in each group. With more samples, the trend might be more obvious. The second limitation is about the wound types. Although we also had iatrogenic wounds, vascular disease-related wounds, infectious wounds, and decubitus, there were no more than 4 samples of each, and the focus was only on the traumatic wounds. So, the result just represented the traumatic wounds. The third is about the diseases that patients had. We collected patients' information, including age, gender, BMI, smoking, and diabetes. But some other conditions, like tumors

and rheumatoid (Xia, Inoue et al. 2022), which can affect the expression of TGF-β, were not included. The last is the immunohistochemistry staining methods, including quantifying positive nucleus percentage. We referred to some quantification methods published, but it was still difficult to calculate accurately, even with manual counting. It will be better to find or combine some other experimental methods in the future.

5. Summary

In this study, patients' samples, including wound tissue and serum, were investigated to explore the possible molecular mechanisms behind chronic wounds. High levels of TGF-β1 were found in wound tissue and serum of patients with chronic wounds. This was not consistent with previous literature. In the following experiments, this result was further confirmed in patients with chronic trauma wounds. The most important finding was that an impaired TGF-β signaling pathway was verified, and endogenous inhibitors on the membrane or in the cytoplasm led to partial inactivation.

Besides the data from the clinic, a new *in vitro* wound model was also established. Similar to real wounds, it could be maintained for 14 days and changed with time. *TGF-β1-3* and its target gene expressions were detectable in this model. After the addition of exogenous TGF-β1-3 separately, different changes happened in the scab stability and target gene expression. Among these three TGF-β isoforms, TGF-β1 showed the most obvious effect on the scab stability and angiogenesis ability. Most of the results were corresponding to the literature. So, this model was available *in vitro* wound model and can be used to track inhibitors and test treatment targets. The plan will focus on these inhibitors to find the treatment target.

This study also has its limitations, such as the small number of patient samples, wound types, and experimental methods. For the wound model, only one type of skin cell was used in this co-culture model. In the future, finding a way to solve these limitations will be very significant.

6. Zusammenfassung

In dieser Studie wurden Patientenproben, darunter Wundgewebe und Serum, untersucht, um die möglichen molekularen Mechanismen hinter chronischen Wunden zu untersuchen. Im Wundgewebe und im Serum der Patienten wurde ein hoher TGF-β1-Spiegel gefunden. Dies stimmte nicht mit der bisherigen Literatur überein. In den folgenden Experimenten wurde dieses Ergebnis bei Patienten mit chronischen Traumawunden weiter bestätigt. Das wichtigste Ergebnis war, dass ein beeinträchtigter TGF-β-Signalweg identifiziert wurde und endogene Inhibitoren auf der Membran oder im Zytoplasma zu einer teilweisen Inaktivierung führten. Der zukünftige Plan wird sich auf diese Inhibitoren konzentrieren, um das Behandlungsziel zu finden.

Neben den Daten aus der Klinik wurde auch ein neues In-vitro-Wundmodell etabliert. Ähnlich wie bei echten Wunden konnte es 14 Tage lang erhalten bleiben und sich mit der Zeit verändern. TGF-β1-3 und die Expression seiner Zielgene waren in diesem Modell nachweisbar. Nach der separaten Zugabe von exogenem TGF-β1-3 kam es zu unterschiedlichen Veränderungen in der Schorfstabilität und der Zielgenexpression. Unter diesen drei TGF-β-Isoformen zeigte TGF-β1 den offensichtlichsten Effekt auf die Schorfstabilität und die Fähigkeit zur Angiogenese. Und die meisten Ergebnisse entsprachen der Literatur. Dieses Modell war also ein verfügbares In-vitro-Wundmodell und kann zur Verfolgung von Inhibitoren und zum Testen von Behandlungszielen verwendet werden.

Diese Studie weist auch ihre eigenen Einschränkungen auf, wie z. B. die geringe Anzahl an Patientenproben, Wundtypen und experimentellen Methoden. Für das Wundmodell wurde in diesem Co-Kulturmodell nur eine Art von

Hautzellen verwendet. In Zukunft wird es von großer Bedeutung sein, einen Weg zur Lösung dieser Einschränkungen zu finden.

7. Bibliography

Ahn, A. C. and T. J. Kaptchuk (2011). "Spatial anisotropy analyses of subcutaneous tissue layer: potential insights into its biomechanical characteristics." Journal of Anatomy **219**(4): 515-524.

Annes, J. P., et al. (2003). "Making sense of latent TGFbeta activation." J Cell Sci **116**(Pt 2): 217-224.

Ansel, J., et al. (1990). "Cytokine modulation of keratinocyte cytokines." J Invest Dermatol **94**(6 Suppl): 101s-107s.

Barrientos, S., et al. (2008). "Growth factors and cytokines in wound healing." Wound Repair Regen **16**(5): 585-601.

Baum, C. L. and C. J. Arpey (2005). "Normal cutaneous wound healing: Clinical correlation with cellular and molecular events." Dermatologic Surgery **31**(6): 674-686.

Brunner, G. and R. Blakytny (2004). "Extracellular regulation of TGF-beta activity in wound repair: growth factor latency as a sensor mechanism for injury." Thromb Haemost **92**(2): 253-261.

Cabral-Pacheco, G. A., et al. (2020). "The Roles of Matrix Metalloproteinases and Their Inhibitors in Human Diseases." International Journal of Molecular Sciences **21**(24).

Campos, L. D., et al. (2023). "Collagen supplementation in skin and orthopedic diseases: A review of the literature." Heliyon **9**(4): e14961.

Carpentier, G., et al. (2020). "Angiogenesis Analyzer for ImageJ — A comparative morphometric analysis of “Endothelial Tube Formation Assay” and “Fibrin Bead Assay”." Scientific Reports **10**(1): 11568.

Crowe, M. J., et al. (2000). "Delayed Wound Healing in Immunodeficient TGF-β1 Knockout Mice." Journal of Investigative Dermatology **115**(1): 3-11.

Darby, I. A., et al. (2014). "Fibroblasts and myofibroblasts in wound healing." Clin Cosmet Investig Dermatol **7**: 301-311.

Ehnert, S., et al. (2018). "Immune Cell Induced Migration of Osteoprogenitor Cells Is Mediated by TGF-beta Dependent Upregulation of NOX4 and Activation of Focal Adhesion Kinase." International Journal of Molecular Sciences **19**(8).

Ehnert, S., et al. (2023). "Increased Levels of BAMBI Inhibit Canonical TGF-beta Signaling in Chronic Wound Tissues." Cells **12**(16).

Ehnert, S., et al. (2011). "Autologous serum improves yield and metabolic capacity of monocyte-derived hepatocyte-like cells: possible implication for cell transplantation." Cell Transplant **20**(9): 1465-1477.

Falanga, V., et al. (2022). "Chronic wounds." Nature Reviews Disease Primers **8**(1): 50.

Fan, Y., et al. (2015). "BAMBI elimination enhances alternative TGF-β signaling and glomerular dysfunction in diabetic mice." Diabetes **64**(6): 2220-2233.

Ferrari, G., et al. (2009). "Transforming growth factor-beta 1 (TGF-beta1) induces angiogenesis through vascular endothelial growth factor (VEGF)-mediated apoptosis." J Cell Physiol **219**(2): 449-458.

Ferrari, G., et al. (2009). "Transforming growth factor-beta 1 (TGF-β1) induces angiogenesis through vascular endothelial growth factor (VEGF)-mediated apoptosis." Journal of Cellular Physiology **219**(2): 449-458.

Finnson, K. W., et al. (2013). "Dynamics of Transforming Growth Factor Beta Signaling in Wound Healing and Scarring." Adv Wound Care (New Rochelle) **2**(5): 195-214.

Frazier, K., et al. (1996). "Stimulation of fibroblast cell growth, matrix production, and granulation tissue formation by connective tissue growth factor." Journal of Investigative Dermatology **107**(3): 404-411.

Gailit, J., et al. (1994). "TGF-beta 1 stimulates expression of keratinocyte integrins during re-epithelialization of cutaneous wounds." J Invest Dermatol **103**(2): 221-227.

Gifford, C. C., et al. (2021). "Negative regulators of TGF-beta1 signaling in renal fibrosis; pathological mechanisms and novel therapeutic opportunities." Clin Sci (Lond) **135**(2): 275-303.

Gould, L., et al. (2015). "Chronic Wound Repair and Healing in Older Adults: Current Status and Future Research." Journal of the American Geriatrics Society **63**(3): 427-438.

Green, E. M., et al. (2014). "The structure and micromechanics of elastic tissue." Interface Focus **4**(2): 20130058.

Gushiken, L. F. S., et al. (2021). "Cutaneous Wound Healing: An Update from Physiopathology to Current Therapies." Life **11**(7): 665.

Halder, S. K., et al. (2005). "Smad7 induces tumorigenicity by blocking TGF-β-induced growth inhibition and apoptosis." Experimental Cell Research **307**(1): 231-246.

Hartung, T. (2008). "Thoughts on limitations of animal models." Parkinsonism & Related Disorders **14**: S81-S83.

Haussling, V., et al. (2019). "Impact of Four Protein Additives in Cryogels on Osteogenic Differentiation of Adipose-Derived Mesenchymal Stem Cells." Bioengineering-Basel **6**(3).

Hyytiäinen, M., et al. (2004). "Latent TGF-beta binding proteins: extracellular matrix association and roles in TGF-beta activation." Crit Rev Clin Lab Sci **41**(3): 233-264.

Ignotz, R. A. and J. Massague (1986). "Transforming Growth-Factor-Beta Stimulates the Expression of Fibronectin and Collagen and Their Incorporation into the Extracellular-Matrix." Journal of Biological Chemistry **261**(9): 4337-4345.

Järbrink, K., et al. (2016). "Prevalence and incidence of chronic wounds and related complications: a protocol for a systematic review." Syst Rev **5**(1): 152.

Kiritsi, D. and A. Nystrom (2018). "The role of TGF beta in wound healing pathologies." Mechanisms of Ageing and Development **172**: 51-58.

Kolaczkowska, E. and P. Kubes (2013). "Neutrophil recruitment and function in health and inflammation." Nature Reviews Immunology **13**(3): 159-175.

Krstic, J. and J. F. Santibanez (2014). "Transforming growth factor-beta and matrix metalloproteinases: functional interactions in tumor stroma-infiltrating myeloid cells." ScientificWorldJournal **2014**: 521754.

Labler, L., et al. (2006). "[Influence of V.A.C.-therapy on cytokines and growth factors in traumatic wounds]." Zentralbl Chir **131 Suppl 1**: S62-67.

Ladwig, G. P., et al. (2002). "Ratios of activated matrix metalloproteinase-9 to tissue inhibitor of matrix metalloproteinase-1 in wound fluids are inversely correlated with healing of pressure ulcers." Wound Repair Regen **10**(1): 26-37.

Landen, N. X., et al. (2016). "Transition from inflammation to proliferation: a critical step during wound healing." Cell Mol Life Sci **73**(20): 3861-3885.

Lee, J.-H. (2015). Chapter 3 - Keratinocyte Differentiation and Epigenetics. Epigenetics and Dermatology. Q. Lu, C. C. Chang and B. C. Richardson. Boston, Academic Press**:** 37-52.

Li, J., et al. (2003). "Angiogenesis in wound repair: angiogenic growth factors and the extracellular matrix." Microsc Res Tech **60**(1): 107-114.

Lichtman, M. K., et al. (2016). "Transforming growth factor beta (TGF-beta) isoforms in wound healing and fibrosis." Wound Repair Regen **24**(2): 215-222.

Lin, J., et al. (2012). "Comparative analysis of phase I and II enzyme activities in 5 hepatic cell lines identifies Huh-7 and HCC-T cells with the highest potential to study drug metabolism." Arch Toxicol **86**(1): 87-95.

Liu, C., et al. (2022). "Establishment of an In Vitro Scab Model for Investigating Different Phases of Wound Healing." Bioengineering (Basel) **9**(5).

Liu, Y., et al. (2016). "TGF-beta1 promotes scar fibroblasts proliferation and transdifferentiation via up-regulating MicroRNA-21." Sci Rep **6**: 32231.

Lu, P., et al. (2011). "Extracellular matrix degradation and remodeling in development and disease." Cold Spring Harb Perspect Biol **3**(12).

Martin, P. (1997). "Wound healing - Aiming for perfect skin regeneration." Science **276**(5309): 75-81.

Martinengo, L., et al. (2019). "Prevalence of chronic wounds in the general population: systematic review and meta-analysis of observational studies." Ann Epidemiol **29**: 8-15.

Massagué, J. (2000). "How cells read TGF-β signals." Nature Reviews Molecular Cell Biology **1**(3): 169-178.

Mathew-Steiner, S. S., et al. (2021). "Collagen in Wound Healing." Bioengineering (Basel) **8**(5).

Menon, G. K., et al. (2012). "The structure and function of the stratum corneum." Int J Pharm **435**(1): 3-9.

Morikawa, M., et al. (2016). "TGF-β and the TGF-β Family: Context-Dependent Roles in Cell and Tissue Physiology." Cold Spring Harb Perspect Biol **8**(5).

Mu, M., et al. (2019). "Ferulic acid attenuates liver fibrosis and hepatic stellate cell activation via inhibition of TGF-beta/Smad signaling pathway [Corrigendum]." Drug Des Devel Ther **13**: 1819.

Nakao, A., et al. (1997). "Identification of Smad7, a TGF beta-inducible antagonist of TGF-beta signalling." Nature **389**(6651): 631-635.

Pakyari, M., et al. (2013). "Critical Role of Transforming Growth Factor Beta in Different Phases of Wound Healing." Adv Wound Care (New Rochelle) **2**(5): 215-224.

Paola, A. G. and H. M. Joseph (2017). TGF-β Activation and Signaling in Angiogenesis. Physiologic and Pathologic Angiogenesis. S. Dan and S. Agneta. Rijeka, IntechOpen**:** Ch. 1.

Penn, J. W., et al. (2012). "The role of the TGF-beta family in wound healing, burns and scarring: a review." Int J Burns Trauma **2**(1): 18-28.

Pepper, M. S. (1997). "Transforming growth factor-beta: vasculogenesis, angiogenesis, and vessel wall integrity." Cytokine Growth Factor Rev **8**(1): 21-43.

Pfeiffenberger, M., et al. (2019). "Hypoxia and mesenchymal stromal cells as key drivers of initial fracture healing in an equine in vitro fracture hematoma model." Plos One **14**(4): e0214276.

Pfisterer, K., et al. (2021). "The Extracellular Matrix in Skin Inflammation and Infection." Front Cell Dev Biol **9**: 682414.

PIEK, E., et al. (1999). "Specificity, diversity, and regulation in TGF-β superfamily signaling." The FASEB Journal **13**(15): 2105-2124.

Raeder, K., et al. (2020). "Prevalence and risk factors of chronic wounds in nursing homes in Germany A Cross-Sectional Study." International Wound Journal **17**(5): 1128-1134.

Ramirez, H., et al. (2014). "The Role of TGFbeta Signaling in Wound Epithelialization." Adv Wound Care (New Rochelle) **3**(7): 482-491.

Reinke, J. M. and H. Sorg (2012). "Wound Repair and Regeneration." European Surgical Research **49**(1): 35-43.

Reiss, M. J., et al. (2010). "Matrix metalloproteinase-9 delays wound healing in a murine wound model." Surgery **147**(2): 295-302.

Richardson, M. (2004). "Acute wounds: an overview of the physiological healing process." Nurs Times **100**(4): 50-53.

Rivera, A. E. and J. M. Spencer (2007). "Clinical aspects of full-thickness wound healing." Clin Dermatol **25**(1): 39-48.

Roberts, A. B., et al. (1990). "Transforming Growth-Factor-Beta - Major Role in Regulation of Extracellular-Matrix." Annals of the New York Academy of Sciences **580**: 225-232.

Roberts, A. B., et al. (1992). "Tgf-Beta - Regulation of Extracellular-Matrix." Kidney International **41**(3): 557-559.

Roberts, A. B., et al. (2003). "Smad3: a key player in pathogenetic mechanisms dependent on TGF-beta." Ann N Y Acad Sci **995**: 1-10.

Saarialho-Kere, U. K. (1998). "Patterns of matrix metalloproteinase and TIMP expression in chronic ulcers." Arch Dermatol Res **290 Suppl**: S47-54.

Sami, D. G., et al. (2019). "Wound healing models: A systematic review of animal and non-animal models." Wound Medicine **24**(1): 8-17.

Schrementi, M. E., et al. (2008). "Site-specific production of TGF-beta in oral mucosal and cutaneous wounds." Wound Repair Regen **16**(1): 80-86.

Scott, D. W. and W. H. Miller (2003). Chapter 1 - Structure and Function of the Skin. Equine Dermatology. D. W. Scott and W. H. Miller. Saint Louis, W.B. Saunders**:** 1-58.

Secker, G. A., et al. (2008). "TGF beta stimulated re-epithelialisation is regulated by CTGF and Ras/MEK/ERK signalling." Experimental Cell Research **314**(1): 131-142.

Segel, G. B., et al. (2011). "The paradox of the neutrophil's role in tissue injury." Journal of Leukocyte Biology **89**(3): 359-372.

Sen, C., et al. (2017). "Wound Healing (Neligan Plastic Surgery: Volume One)." Published online.

Shaw, T. J. and P. Martin (2016). "Wound repair: a showcase for cell plasticity and migration." Current Opinion in Cell Biology **42**: 29-37.

Shichiri, M. and Y. Hirata (2001). "Antiangiogenesis signals by endostatin." Faseb j **15**(6): 1044-1053.

Shida, N., et al. (2016). "Study of plasma coagulation induced by contact with calcium chloride solution." Soft Matter **12**(47): 9471-9476.

Taylor, A. W. (2009). "Review of the activation of TGF-beta in immunity." J Leukoc Biol **85**(1): 29-33.

Tracy, L. E., et al. (2016). "Extracellular Matrix and Dermal Fibroblast Function in the Healing Wound." Adv Wound Care (New Rochelle) **5**(3): 119-136.

Velickovic, V. M., et al. (2022). "Cost-effectiveness analysis of superabsorbent wound dressings in patients with moderate-to-highly exuding leg ulcers in Germany." International Wound Journal **19**(2): 447-459.

Velnar, T., et al. (2009). "The Wound Healing Process: an Overview of the Cellular and Molecular Mechanisms." Journal of International Medical Research **37**(5): 1528-1542.

Verrecchia, F. and A. Mauviel (2007). "Transforming growth factor-beta and fibrosis." World J Gastroenterol **13**(22): 3056-3062.

Vinals, F. and J. Pouyssegur (2001). "Transforming growth factor beta1 (TGF-beta1) promotes endothelial cell survival during in vitro angiogenesis via an autocrine mechanism implicating TGF-alpha signaling." Mol Cell Biol **21**(21): 7218-7230.

Volpert, O. V., et al. (1998). "Inhibition of angiogenesis by interleukin 4." J Exp Med **188**(6): 1039-1046.

Wager, L. and D. Leavesley (2015). "MicroRNA regulation of epithelial-to-mesenchymal transition during re-epithelialisation: assessing an open wound." Wound Practice & Research: Journal of the Australian Wound Management Association **23**(3): 132-142.

Witte, M. B. and A. Barbul (1997). "General principles of wound healing." Surg Clin North Am **77**(3): 509-528.

Worthington, J. J., et al. (2011). "TGFbeta: a sleeping giant awoken by integrins." Trends Biochem Sci **36**(1): 47-54.

Xia, Y., et al. (2022). "TGFbeta reprograms TNF stimulation of macrophages towards a non-canonical pathway driving inflammatory osteoclastogenesis." Nat Commun **13**(1): 3920.

Yang, L., et al. (1999). "Active transforming growth factor-beta in wound repair: determination using a new assay." Am J Pathol **154**(1): 105-111.

Young, A. and C.-E. McNaught (2011). "The physiology of wound healing." Surgery (Oxford) **29**(10): 475-479.

Yousef, H., et al. (2022). Anatomy, Skin (Integument), Epidermis. StatPearls. Treasure Island (FL), StatPearls Publishing Copyright © 2022, StatPearls Publishing LLC.

Yousef, H. and s. Sharma (2017). Anatomy, Skin (Integument), Epidermis.

Yuan, Q., et al. (2022). "A Klotho-derived peptide protects against kidney fibrosis by targeting TGF-beta signaling." Nat Commun **13**(1): 438.

Zeng, Q., et al. (2017). 6.20 Skin Tissue Engineering☆. Comprehensive Biomaterials II. P. Ducheyne. Oxford, Elsevier**:** 334-382.

Zhang, R., et al. (2019). Power Distribution and Performance Analysis of Terahertz Communication in Artificial Skin.

Zhang, T., et al. (2020). "Current potential therapeutic strategies targeting the TGF-β/Smad signaling pathway to attenuate keloid and hypertrophic scar formation." Biomed Pharmacother **129**: 110287.

Zimmerman, A., et al. (2014). "The gentle touch receptors of mammalian skin." Science **346**(6212): 950-954.

Beyene, R. T., et al. (2020). "The Effect of Comorbidities on Wound Healing." Surg Clin North Am **100**(4): 695-705.

Chung, J. Y., et al. (2021). "TGF-β Signaling: From Tissue Fibrosis to Tumor Microenvironment." International Journal of Molecular Sciences **22**(14).

Ehnert, S., et al. (2023). "Increased Levels of BAMBI Inhibit Canonical TGF-β Signaling in Chronic Wound Tissues." Cells **12**(16).

Eyerich, S., et al. (2018). "Cutaneous Barriers and Skin Immunity: Differentiating A Connected Network." Trends in Immunology **39**(4): 315-327.

Frykberg, R. G. and J. Banks (2015). "Challenges in the Treatment of Chronic Wounds." Adv Wound Care (New Rochelle) **4**(9): 560-582.

Hofmann, E., et al. (2023). "Human In Vitro Skin Models for Wound Healing and Wound Healing Disorders." Biomedicines **11**(4).

Karamichos, D., et al. (2009). "An experimental model for assessing fibroblast migration in 3-D collagen matrices." Cell Motil Cytoskeleton **66**(1): 1-9.

Liu, C., et al. (2022). "Establishment of an In Vitro Scab Model for Investigating Different Phases of Wound Healing." Bioengineering (Basel) **9**(5).

Renner, R. and C. Erfurt-Berge (2017). "Depression and quality of life in patients with chronic wounds: ways to measure their influence and their effect on daily life." Chronic Wound Care Management and Research **Volume 4**: 143-151.

Richmond, N. A., et al. (2013). "Evidence-based management of common chronic lower extremity ulcers." Dermatol Ther **26**(3): 187-196.

Ud-Din, S. and A. Bayat (2017). "Non-animal models of wound healing in cutaneous repair: In silico, in vitro, ex vivo, and in vivo models of wounds and scars in human skin." Wound Repair Regen **25**(2): 164-176.

Wilkinson, H. and M. Hardman (2020). "Wound healing: cellular mechanisms and pathological outcomes." Open Biology.

8. Declaration

This study was performed entirely at Siegfried Weller Institute under the guidance of Prof. Dr. Andreas Nüssler and Prof. Dr. Sabrina Ehnert.

All experiments were completed by me. The establishment of *in vitro* scab was performed with the help of Helen Rinderknecht. Melanie Voss prepared paraffin sections. Immunohistochemistry staining and Western blot were completed with the help of Caren Linnemann. Tube formation assay and angiogenesis array were done with the help of Chao Lu and Helen Rinderknecht.

All the data analysis was completed under the guidance of Prof. Dr. Sabrina Ehnert.

All presented data are derived from our original work, except for the quoted references and figures. Also, two figures from other papers have permission licenses.

I hereby declare that the submitted thesis entitled: “Chronic wounds are associated with inhibition of Smad3 phosphorylation” has been written by myself. This work has not been submitted in any application for a degree.

9. Publication

The results of this thesis were partially used for publication:

Title:

Establishment of an In Vitro Scab Model for Investigating Different Phases of Wound Healing

Author:

Chao Liu, Helen Rinderknecht, Tina Histing, Jonas Kolbenschlag, Andreas K Nussler, Sabrina Ehnert

Journal:

Bioengineering (Basel) 2022 Apr 28;9(5):191.

doi: 10.3390/bioengineering9050191

Title:

Increased Levels of BAMBI Inhibit Canonical TGF-β Signaling in Chronic Wound Tissues

Author:

Ehnert S, Rinderknecht H, Liu C, Voss M, Konrad FM, Eisler W, Alexander D, Ngamsri KC, Histing T, Rollmann MF, Nussler AK.

Journal:

Cells 2023 Aug 18;12(16):2095.

doi: 10.3390/cells12162095.

10. Acknowledgement

I want to express my profound appreciation to my supervisor Prof. Dr. Sabrina Ehnert. This endeavor would not have been possible without her guidance, her expertise, suggestion, and invaluable encouragement. I am also deeply grateful to Prof. Dr. Andreas Nüssler for his motivation and advice. His working attitude, especially in combining basic research with clinical work, encouraged me a lot.

I am also deeply grateful to Prof. Dr. Robert Lukowski and Prof. Dr. Manuel Held, in my doctoral committee, who have generously provided helpful suggestions with their broad knowledge and expertise.

I also want to express my special thanks to Dr. Inka Montero and Dr. Lina Maria Bandholz-Cajamarca for their patience and considerate help and instructions in so many situations during my whole Ph.D. program.

I sincerely thank my colleagues Bianca Braun, Caren Linnemann, Helen Rinderknecht, Romina Apsera-Werz, Regina Breinbauer and Svetlana Gasimova for excellent teaching and warm help.

Thanks to my Chinese colleagues at the SWI, Yangmengfan Chen, Tao Chen, Chao Lu, Weidong Weng, Sheng Zhu and Sanhuan Yuan; they helped me a lot and set a good example for me.

I want to thank my friends who have always supported me, whether in China or Germany.

Last, I am incredibly grateful to my beloved family for their sacrifice and support over these years.